COMPUTATIONAL CANOPY MODELS FOR PRECISION MEASUREMENT AND ADAPTIVE MANAGEMENT OF GRAPEVINE PERFORMANCE

A Dissertation

Presented to the Faculty of the Graduate School

of Cornell University

In Partial Fulfillment of the Requirements for the Degree of

Doctor of Philosophy

by

James Matthew Meyers

January 2011

COMPUTATIONAL CANOPY MODELS FOR PRECISION MEASUREMENT AND ADAPTIVE MANAGEMENT OF GRAPEVINE PERFORMANCE

James Matthew Meyers, Ph. D.

Cornell University 2011

Effective control of winegrape fruit quality requires the simultaneous consideration of multiple response models including: the relationship between the chemical profile of harvested fruit and the organoleptic qualities of a finished wine; a mechanistic understanding of key flavor and aroma compound biosynthesis; and the role of physical vineyard parameters in these biosynthetic processes. Any attempt to predictably influence the performance of a winegrape cropping system, with respect to flavor and aroma, requires the ability to both measure the relevant physical parameters of that system and to accurately manipulate them to achieve a deliberate and quantitative response. Although the sub-discipline of *precision viticulture* has established that a quantitative understanding of plot-scale spatial variability can guide cultural inputs toward plot-scale consistency, the existence and small-scale spatial patterns and their effect on precision management have not been extensively studied. The experiments presented here were designed to: 1) improve the precision and increase the spatial resolution of commonly used viticultural research methods with the goal of identifying, characterizing and quantifying small-scale spatial patterns in fruiting-zone of winegrape canopies; 2) explore the impact of small-scale spatial structure on the efficacy of common plot-level cultural inputs; 3) develop methods for optimizing vineyard research and commercial production operations within known parametric spatial patterns at multiple scales; and, 4) explore the potential application

of these methods in the control of a specific sunlight-sensitive compound vital to the organoleptic qualities of Riesling wine. The development and application of new computational methods for managing both the data volume of high-resolution models and the combinatorial complexities of multi-objective vineyard optimization, resulted in: new quantitative metrics for describing fruit-zone sunlight regimes; the discovery and quantification of small-scale culturally-induced microclimatic spatial patterns; the discovery that small-scale spatial patterns can negatively impact the efficacy of plot-scale cultural inputs; and an enhanced understanding of the relationship between canopy microclimatic variability and concentrations of C13-norisoprenoids in Riesling grapes. To date, the software tools developed within the scope of dissertation have been adopted by researchers and winegrape growers in a dozen countries and 14 U.S. states for use in the study and optimization of crop performance and fruit metabolite profiles.

BIOGRAPHICAL SKETCH

James Meyers was born in Illinois and lived in a half-dozen additional states before settling in New York. Along the way, he earned a B.S. in Chemistry & Biology from West Chester University of Pennsylvania (1990) and an M.S. in Computer Science from Brown University (1992). Prior to studying at Cornell, James served as Chief Executive Officer of a software automation company that he co-founded in the 1990s.

Dedicated to reality – the mother of all delusions.

ACKNOWLEDGMENTS

This dissertation would not exist without innumerable external contributions and influences. Central to these sources of ideas, inspirations, and support were my committee members; each of whom shaped my experiences, research, and successes in a unique manner. Foremost, I would like to thank Dr. Justine Vanden Heuvel for her resolute support and encouragement of my often unconventional approaches to viticultural systems. Her willingness to entertain the practical merits of new models, no matter how unusual, fueled my confidence, energy and persistence. Evidence needed to gauge the influence of our results awaits the passage of time, but Justine's readiness to work "outside of the box" is, in my opinion, deserving of immediate applause and emulation. I would also like to acknowledge: Dr. Gavin Sacks for his endless intellectual curiosity, good humor, patience, and steadfast defense of reality; Dr. Harold van Es for introducing me to the hidden patterns within agricultural systems, thereby strengthening my position in the battle against entropy; and Dr. Wayne Wilcox for demonstrating that there are no limits to either the quantity or quality of what an individual can accomplish if they are having fun doing it.

As a Ph.D. student Cornell, I participated in approximately two dozen courses, mostly in the role of student, but also often as a teaching assistant. Each of these courses has influenced my work, and I would like to specifically acknowledge Dr. Alan Lakso for illuminating the enormous value in seeking quantitative mechanistic explanations for physiological responses; Dr. Ramón Mira de Orduña for honestly and thoroughly framing commercial wine production in the context of a complex industrial process; and Dr. Christine Shoemaker for reminding me that complex industrial processes, especially those whose variables can be defined in a mechanistic manner, can be optimized – regardless of their dimensional complexity.

My classroom experiences occasionally transcended the simple acquisition of facts and scientific concepts by offering inspirational exemplars of professional and personal excellence. In the relentless pursuit of research objectives, it is easy to overlook the central importance of classroom education and student-professor relationships within the broader framework of human achievement. For this reason, I would like to acknowledge Kathy Arnik, Dr. Steve DeGloria, Dr. Ian Merwin, Dr. Gavin Sacks, and Dr. Tom Silva for their extraordinary commitments to students and education.

I would also like to offer thanks to my fellow lab members and collaborators for their camaraderie, personal perspectives, and invaluable assistance – particularly for the sociological assistance from my fellow "non-traditional" colleagues: Misha Kwasniewski, Trent Preszler and Justin Scheiner; and to Steve Lerch for reminding me that, although there are over six billion people on this planet, each of us is uniquely valuable. My apologies for the inevitable oversight, as I try to recall the many other people who have provided needed assistance, guidance, and distraction over the years: Vinny Aliperti, Craig Austin, Nina Bassuk, Terry Bates, Chaz Coney, Peter Cousins, Craig Cramer, Ted Fulkerson, Matt Gates, Ben Gavitt, Chris Gerling, Eric Hazlitt, Jim Hazlitt, Tina Hazlitt, Dolores Higareda, Diego Intrigliolo, Meera Iyer, Michelle Leinfelder, Tian Ling, Anna Katherine Mansfield, Paul Martin, Tim Martinson, Michelle Moyer, Rebecca Nelson, Bruce Pan, Vinay Pagay, Hans Walter-Peterson, Luann Preston-Wilsey, Marvin Pritts, Lou Ann Rago, Pam Raes, Michelle Rose, Imelda Ryona, Piero Spada, Qun Sun, Rob Thomas, Sue Thompson, Mark Wagner, John Wagner, Max Welcome, Josh Wig, Bill Wilsey, and Wendy Wirth.

Finally, and most importantly, I wish to thank my wife Rosemary for her endless understanding, support, and encouragement. Her cheerful accommodation of my obsessions is a phenomenon beyond scientific explanation.

TABLE OF CONTENTS

LIST OF FIGURES

LIST OF TABLES

CHAPTER 1

ENHANCING THE PRECISION AND SPATIAL ACUITY OF POINT QUADRAT ANALYSES VIA CALIBRATED EXPOSURE MAPPING

Abstract: Modeling canopy sunlight environments requires precise measurements of biomass distribution and photon flux distribution (PFD). However, customary methods for obtaining these measurements are limited in their precision and practicality. Point quadrat analysis (PQA), the standard for canopy architecture, is limited in spatial precision and the lack of calibration; while measurement of PFD across an entire canopy typically requires rigorous sampling protocols. This paper introduces new methods that combine PQA and photon flux measurements into a calibrated biomass and PFD model. These techniques, applied to sample data from a shoot thinning study, revealed quantitative descriptions of canopy biomass distribution, light environment and treatment efficacy.

Key words: Light attenuation, light interception, biomass distribution, canopy management, shoot thinning

Introduction

Sunlight intensity in a grapevine canopy fruiting zone has been shown to strongly correlate with key fruit composition measures such as sugars, acids, and a variety of secondary metabolites involved in wine flavors and aromas, including phenolics (Downey et al. 2006), monoterpenes (Reynolds and Wardle 1989), norisoprenoids (Lee et al. 2007), and methoxypyrazines (Hashizume and Samuta 1999). Accordingly, many viticultural treatments associated with canopy management

are intended to manipulate the photosynthetic photon flux (PPF) of the fruiting zone or the distribution of photon flux across the total leaf area of the canopy to achieve metabolic effect.

To establish the efficacy of viticultural treatments, researchers compare pre- and post-treatment measurements of specific microclimatic indicators and look for correlations between those differences and both quantitative and qualitative harvest data. Point quadrat analysis (PQA) has been used for decades as a method for measuring and comparing microclimatic indicators of a canopy, including canopy consistency, leaf area density, cluster exposure, and leaf area source/sink balance (i.e., exterior vs. interior leaves) (Smart and Robinson 1991). PQA has been used to characterize both vertically shoot positioned and non-vertically positioned trellis systems (Gladstone and Dokoozlian 2003). PPF is commonly measured directly via a ceptometer placed at the location of interest. Both PQA and direct PPF measurement are relatively simple and easily performed, but they have limitations. For example, optimal viticultural practices should be guided by precise sunlight measurements at multiple locations within the canopy, but PPF measurements are often limited to the fruiting zone. This is because it is an important location, but also because it is easy to define and locate. Obtaining PPF readings at other points in the canopy requires establishing a rigorous coordinate system within the canopy and recording a considerably larger number of samples (Schultz 1995). Sampling a large number of PPF values is potentially error prone because of the shifting sun location and variable cloud cover during lengthy data collection.

Numerical analysis methods traditionally associated with PQA underutilize the spatial information collected by defining individual leaf or cluster exposure as a binary function: exposed (not interior) or unexposed (interior) (Smart and Robinson 1991). This approach presupposes that all interior leaves and clusters are equally exposed to

sunlight, or that the differences in exposure are immaterial. This approach to exposure analysis diminishes precision, and thus reduces the confidence of efficacy correlations offered by PQA-based viticultural research. More elaborate methods of describing leaf area density (Schultz 1995, Gladstone and Dokoozlian 2003) have been attempted which can depict the asymmetrical spatial distribution of biomass within the canopy, but the implementation of these methods is relatively difficult and time consuming.

New methods for using the previously ignored spatial information collected from PQA datasets, and for simplifying whole-canopy PPF sampling protocols, have been developed and are described in this paper. Some of the proposed methods expand on traditional PQA analyses by enhancing numerical methods to compute leaf and cluster exposure as a continuous function and by introducing metrics for expressing biomass symmetry. Other methods integrate a minimal number of PPF measurements with traditional PQA data into a computational model designed to establish a calibrated canopy photon flux attenuation curve, and to produce maps of leaf and cluster exposures without the need for extensive PPF sampling. These new methods are demonstrated through a sample data set from a shoot-thinning study. All new spatial and calibrated flux metrics, discussed in the next section, are summarized in Table 1.1.

Table 1.1. Summary of new point quadrat analysis metrics

Metric	Abbreviation	Units of Expression	Value Range	Description
Occlusion layer number	OLN	Contacts	1 to infinity	Number of shade-producing contacts (leaves and clusters) per insertion
Cluster exposure layer	CEL	Occlusion layers	0 to infinity	Number of shading layers between clusters and the nearest canopy boundary
Leaf exposure layer	LEL	Occlusion layers	0 to infinity	Number of shading layers between leaves and the nearest canopy boundary
Canopy cluster symmetry	CCS	None	-1 to 1	The ratio of the number of occlusion layers between a cluster and the insertion side of the canopy versus the exit side of the canopy. A value of 0 indicates that the distances are equal. A negative value indicates that clusters are biased to the exit side (– (1 – exit / insertion)). A positive value indicates that the bias is toward the insertion side (1 – (insertion/exit)).
Canopy calibration coefficient	Ep1	None	0 to 1	The average percentage, expressed as a decimal, of light that is transmitted beyond an occlusion layer of the canopy.
Cluster exposure flux availability	CEFA	None	0 to 1	The percentage, expressed as a decimal, of above-canopy photon flux that reaches clusters.
Cluster exposure flux symmetry	CEFS	None	-1 to 1	The ratio of the photon flux that clusters receive from the insertion side of the canopy versus the exit side. A value of 0 indicates that the flux is equal. A negative value indicates that flux is biased to the exit side (– (1 – exit/insertion)). A positive value indicates that the bias is toward the insertion side (1 – (insertion / exit)).
Leaf exposure flux availability	LEFA	None	0 to 1	The percentage, expressed as a decimal, of above-canopy photon flux that reaches leaves.
Leaf exposure flux symmetry	LEFS	None	-1 to 1	The ratio of the photon flux that leaves receive from the insertion side of the canopy versus the exit side. A value of 0 indicates that the flux is equal. A negative value indicates that flux is biased to the exit side (– (1 – exit / insertion)). A positive value indicates that the bias is toward the insertion side (1 – (insertion / exit)).
Trellis contact symmetry	TCS	None	-1 to 1	The ratio of the number of biomass contacts on the insertion side of the trellis center, versus the exit side of the trellis center. A value of 0 indicates that the contact counts are equal. A negative value indicates that biomass is biased to the exit side (– (1 – exit/insertion)). A positive value indicates that the bias is toward the insertion side (1 – (insertion / exit)).

Materials and methods

Sample dataset. Sample data to demonstrate the proposed new PQA metrics were obtained from a 16-row block of Vignoles (*Vitis* sp.) at a commercial vineyard in Hector, NY (Finger Lakes region, east side of Seneca Lake). Vines were planted in north-south row orientation, trained to high wire umbrella, and managed according to standard viticultural practices for hybrid canopies in the Finger Lakes region. Half of the vines in the block were shoot thinned to a target of 20 shoots per linear canopy row meter in a replicated fashion, while the remaining (control) vines averaged 24 shoots per linear meter of canopy.

Canopy biomass characterization. Point quadrat analysis was performed pre-veraison in mid-July by inserting a thin metal rod into the fruiting zone along the transverse axis of the canopy row, as described by Smart and Robinson (1991). A tape measure was used as a guide for insertions, which were made at 20-cm intervals along the length of the four-vine panel at the height of the fruiting wire, resulting in a total of 36 insertions per panel.

Photon flux measurements. A Decagon AccuPAR LP-80 photosynthetically active radiation sensor (Decagon Devices, Pullman, WA) was used to measure PPF. Ambient flux was measured above each data panel by averaging 10 flux samples collected over a period of approximately 10 seconds. For the ambient measurements, the ceptometer sensor bar was oriented parallel to the ground, with the sensors facing directly upwards toward the sky. Intra-canopy photon flux was measured by placing the ceptometer inside the canopy with the sensor bar aligned with the longitudinal axis of the row, and the sensors facing directly upwards toward the sky. Sensor height was the same height used for PQA measurements, and sensor depth was the transverse axis (center) of the trellising system. In practice, this depth equated to the location of the cordon wire. The in-canopy flux of each vine was measured by averaging 10 flux

samples, from a single location, collected over a period of approximately 10 seconds. %PPF for each vine's center was determined by dividing the average vine canopy flux measurement by the ambient flux measurement for the panel, and multiplying by 100. Measurements were recorded with the ceptometer bar set to sensor averaging mode.

Continuous functions for cluster and leaf exposure. The standard PQA metrics for sunlight exposure, PIC and PIL, are binary functions through which clusters and leaves are categorized as being either interior to the canopy or not interior to the canopy. Three new metrics were developed to provide a continuous analog measure of exposure. The first, occlusion layer number (OLN), is the total number of leaf and cluster contacts for an insertion sample. The purpose of OLN is to formalize the idea that all canopy contacts contribute to canopy density (Reynolds et al. 1994, 1996), and thus, create shade in the canopy. OLN is a measure of the overall shade-producing biomass density of the canopy, and was calculated as follows,

$$\mathrm{OLN} = \frac{\text{Leaf contacts} + \text{Cluster contacts}}{\text{Insertion count}} \qquad \text{Eq. 1}$$

Clusters and leaves at the second position in a PQA insertion are partially exposed to sunlight (Reynolds et al. 1994). We developed new metrics that determine the distance, in occlusion layers, of a leaf or cluster to the nearest canopy boundary. For a given set of PQA data, the new functions, cluster exposure layer (CEL) and leaf exposure layer (LEL), were calculated as follows:

$$\mathrm{CEL} = \frac{\sum \mathrm{Min}\left\{\begin{matrix}\text{Cluster position} - 1 \\ \text{OLN of insertion} - \text{Cluster position}\end{matrix}\right.}{\text{Total cluster contacts}} \qquad \text{Eq. 2}$$

$$\mathrm{LEL} = \frac{\sum \mathrm{Min}\left\{\begin{matrix}\text{Leaf position} - 1 \\ \text{OLN of insertion} - \text{Leaf position}\end{matrix}\right.}{\text{Total leaf contacts}} \qquad \text{Eq. 3}$$

The 'Min' expression in Eq. 2 and Eq. 3 denotes that the smaller of the two

values was used in the calculation. The first parameter in the expression computes the distance of the leaf or cluster to the PQA insertion side of the canopy, while the second parameter calculates the distance to the PQA exit side of the canopy. In determining the distance to the canopy boundary, both cluster and leaf contacts are counted. In computing CEL for a dataset, the distance from the canopy boundary for each contact was individually computed, added to a running total, and divided by the total number of cluster contacts. In computing LEL for a dataset, the distance from the canopy boundary for each contact was individually computed, added to a running total, and divided by the total number of leaf contacts. A leaf or cluster at either the insertion or exit canopy boundary was considered to be at exposure layer zero (i.e., on the exterior of the canopy). Canopy gaps were not included in either CEL or LEL calculations. Gaps are often localized (i.e. not evenly distributed) in the canopy, and thus, would inappropriately skew the CEL and LEL values of the denser canopy portions.

Canopy biomass symmetry. Cluster canopy symmetry (CCS) was developed to further enhance the precision of the exposure analysis by computing the positional bias of clusters within the canopy. CCS was expressed as a number between -1 and 1, with a value of 0 for a set of PQA insertion data indicating that clusters were equally balanced between their distance, in canopy layers, to insertion side of the canopy and the exit side of the canopy. A hypothetical CCS value of 1 would indicate that all clusters are located exactly at the insertion side boundary of the canopy, while a value of -1 would indicate that all clusters were located exactly at the exit side boundary of the canopy. The CCS metric was designed to characterize the distribution of biomass along the transverse axis of the canopy. By quantifying this symmetry, CCS enables researchers to integrate any available temporal flux data related to the local solar zenith angle and row orientation. CCS was calculated as follows:

$$CCS = \begin{cases} 1 - \left(\frac{\sum(OLN - CEL - 1)}{\sum CEL}\right), \text{ where } \sum CEL > \sum(OLN - CEL - 1) \\ -\left[1 - \left(\frac{\sum CEL}{\sum(OLN - CEL - 1)}\right)\right], \text{ where } \sum CEL \leq \sum(OLN - CEL - 1) \end{cases} \quad \text{Eq. 4}$$

The expression, OLN – CEL – 1, computes the number of shading layers between a cluster and the farthest canopy boundary.

Calculating the positional bias of leaves required a different approach, because there are many more leaves and they have more influence, versus clusters, on the light environment in the canopy. Because leaves account for most of the contacts in a PQA dataset, they are inherently symmetric within the set. We determined that computing leaf symmetry using an LEL-based variant of Eq. 4 would generally produce numbers very close to zero because the midpoint of the average leaf-dominated PQA insertion sample has an equal number of leaves on either side. This does not necessarily mean that the leaves are symmetrically arranged around the centerline of the canopy.

As an alternative to calculating a self-referential symmetry for leaf contacts we developed a metric to calculate biomass symmetry with respect to the intended centerline of the trellising system. By including the trellising system centerline in PQA insertion data (using ‘W’ to record the location of the wire), we calculated the Trellis Contact Symmetry (TCS). TCS, also expressed as a number between -1 and 1, was developed to provide a measurement of trellis consistency and the efficacy of cultural practices intended to maintain a symmetric vine row. TCS was also intended to reveal thigmomorphogenetic responses to local weather phenomena or other environmental stressors (Tarara et al. 2005). Designed as a measure of consistency, TCS is intended to be used in standard deviation calculations. For example, a vineyard could have a mean TCS of zero, but still have high variability from panel to panel or row to row. This variability would be revealed in the standard deviation of the TCS values. TCS

was calculated as follows:

$$\mathrm{TCS} = \begin{cases} 1 - \left(\frac{\sum \mathrm{Contacts}_{\mathrm{exit}}}{\sum \mathrm{Contacts}_{\mathrm{insertion}}}\right), \text{where } \sum \mathrm{Contacts}_{\mathrm{insertion}} > \sum \mathrm{Contacts}_{\mathrm{exit}} \\ -\left[1 - \left(\frac{\sum \mathrm{Contacts}_{\mathrm{insertion}}}{\sum \mathrm{Contacts}_{\mathrm{exit}}}\right)\right], \text{where } \sum \mathrm{Contacts}_{\mathrm{insertion}} \leq \sum \mathrm{Contacts}_{\mathrm{exit}} \end{cases} \quad \text{Eq. 5}$$

The use of traditional PQA calculations (Smart and Robinson 1991) and the new spatial calculations on three example insertions are shown in Table 1.2.

Table 1.2. Traditional PQA exposure metrics and new spatial metrics for three sample insertions. L=leaf, C=cluster, W=wire, G=gap. Values presented are for demonstration purposes and do not relate to the sample data set.

Sample PQA Insertion Data	Traditional Metrics				New Metrics				
	LLN	PIC	PIL	PG	OLN	CEL	LEL	CCS	TCS
LLWCLL G LLWLLCL	3[a]	100[b]	55.55[c]	33%[d]	3.67[e]	1.5[f]	0.78[g]	-0.5[h]	-0.43[i]

[a] On average, the canopy had three layers of leaves from insertion to exit side.
[b] 100% of clusters in the canopy insertions were partially or fully shaded.
[c] 55.55% of leaves in the canopy insertions were partially or fully shaded.
[d] 33% of the canopy insertions made no biomass contact (gap in canopy).
[e] On average, the canopy insertions had 3.67 layers of shading biomass (clusters and leaves). Shoots are not included in OLN.
[f] On average, there were 1.5 layers of shading biomass (leaves and clusters) between the exterior of the canopy and a cluster.
[g] On average, there were 0.78 layers of shading biomass (leaves and clusters) between the exterior of the canopy and a leaf.
[h] On average, clusters were positioned closer to the exit side of the PQA insertions. Specifically, that there were 50% fewer shading layers between clusters and the exit side of the canopy, vs. the insertion side of the canopy.
[i] On average, leaves and clusters were positioned closer to the exit side of the PQA insertions. Specifically, 43% of biomass is on the insertion side of the trellising wire. Note, that TCS can only be calculated if 'W' is recorded with the PQA insertion data; [j] PQA, LLN, PIC, PIL, PG, OLN, CEL, LEL, CCS, TCS: point quadrat analysis, leaf layer number, percent interior clusters, percent interior leaves, percent gaps, occlusion layer number, cluster exposure layer, leaf exposure layer, canopy cluster symmetry, and trellis canopy symmetry, respectively.

Calibration of light attenuation. Light attenuation in grapevine canopies has been shown to have an exponential relationship to canopy depth when depth is expressed as either absolute distance (Dokoozlian and Kliewer 1995a,b) or as a function of LLN (Smart 1985). This implies that the general shape of the light attenuation curve for any given canopy is exponential with respect to PQA exposure layer. With the goal of maximally leveraging the spatial precision of CEL and LEL, we developed a field method for calibrating the light attenuation curve of a canopy. By assuming that the acceleration of attenuation across occlusion layers is approximately constant, we determined that the PPF exposure at a given insertion position can be calculated as:

$$E_{P_{\text{Exposure layer}}} = \left(E_{P_1}\right)^{\text{Exposure layer}} \qquad \text{Eq. 6}$$

where $Ep_{\text{Exposure layer}}$ represents the percentage of above-canopy PPF (%PPF) that has

reached a given exposure layer, and where Ep_1 , or the canopy calibration coefficient, represents the percentage of light that is transmitted across each canopy occlusion layer. For example, an Ep_1 value of 0.34 indicates that each occlusion layer in the canopy blocks 66% of sunlight, while allowing the remaining 34% (a combination of sun flecks and light transmitted through leaves) to reach the next layer. Every canopy will possess a unique rate of attenuation due to its particular canopy architecture and Ep_1 value, which is influenced by innumerable variables including cultivar, nutritional status, and cultural practices.

Since Ep_1 represents a constant acceleration of attenuation, a canopy can be calibrated by fitting the n^{th} root curve with only two known points. The first point, 100% transmittance at occlusion layer zero, is fixed for all canopies. To locate a second point, %PPF was measured directly in the canopy. Rearranging Eq.6 yielded,

$$E_{P_1} = E_{P_x}^{\left(\frac{1}{x}\right)}, \text{where x is any canopy layer} \qquad \text{Eq. 7}$$

Although Ep_1 is equal to the transmittance at occlusion layer one, we determined that it was not practical to attempt to measure it directly because occlusion layer one, or any other fixed integer occlusion layer, cannot be reliably located for flux sampling. We avoided the need to locate a specific canopy layer by sampling %PPF at the longitudinal midline of the canopy. On average, the longitudinal midline of the canopy is half of the distance between the PQA insertion side and exit side of the canopy. Thus, the longitudinal midline can be said to be at OLN / 2. Applying the %PPF measurements at OLN / 2 to Eq. 7 yielded,

$$E_{P_1} = \left(E_{P_{OLN/2}}\right)^{\left(\frac{1}{OLN/2}\right)} \qquad \text{Eq. 8}$$

Photon flux measured at the center of the canopy is the sum of sunlight penetrating from both sides of the row; therefore, Ep_1 was calculated using one half of the %PPF value measured at position OLN/2. The final expression for calculating Ep1 was,

$$E_{P_1} = \left(\frac{E_{P_{OLN/2}}}{2}\right)^{\left(\frac{1}{OLN/2}\right)} \quad \text{Eq. 9}$$

To incorporate this bilateral approach, Eq. 6 was updated to independently calculate the PPF from either side of the canopy, as follows:

$$E_{P_{Exposure\ layer}} = \left(E_{P_1}\right)^{Exposure\ layer} + \left(E_{P_1}\right)^{OLN-Exposure\ layer-1} \quad \text{Eq.10}$$

Biomass exposure mapping. Following from OLN, CEL, LEL, and Ep_1, additional metrics were developed to determine %PPF for any given leaf or cluster in a canopy. Cluster exposure flux availability (CEFA) and leaf exposure flux availability (LEFA) express %PPF of a given PQA dataset. CEFA and LEFA follow from Eq. 10 and were computed as follows:

$$CEFA = \frac{\sum(E_{P_1})^{CEL} + \sum(E_{P_1})^{OLN-CEL-1}}{\text{Total cluster contacts}} \quad \text{Eq. 11}$$

$$LEFA = \frac{\sum(E_{P_1})^{LEL} + \sum(E_{P_1})^{OLN-LEL-1}}{\text{Total leaf contacts}} \quad \text{Eq. 12}$$

Exposure maps, depicting distribution of %PPF values among cluster and leaf contacts, were created by calculating CEFA and LEFA values for each contact in the PQA dataset (Figures 1.1 and 1.2).

Cluster exposure flux symmetry (CEFS) and leaf exposure flux symmetry (LEFS) were developed to provide calibrated PPF symmetry metrics that are

analogous to CCS. CEFS and LEFS represent the symmetry of PPF received by clusters and leaves from either side of the canopy row. Like CCS, CEFS and LEFS were expressed as a number between -1 and 1, where a CEFS value of 0 for a set of PQA insertion data indicated that clusters were receiving an equal amount of photon flux from both sides of the canopy. A hypothetical CEFS value of 1 would indicate that all clusters in the dataset received all of their PPF from the insertion side of the canopy, while a value of -1 would indicate that all clusters received all of their photon flux from sunlight from the exit side of the canopy.

CEFS and LEFS were designed to enable the integration of temporal flux data related to the local solar zenith angle and row orientation. For example, if mesoclimatic data was on hand indicating that the block received 10% more sunlight on the canopy exit side, a grower would probably assume that clusters were receiving more light from that canopy side. By calculating CEFS, true bias in cluster exposure symmetry can be calculated. CEFS was defined as follows,

$$\mathrm{CEFS} = \begin{cases} 1 - \left(\frac{\sum \mathrm{CEFA_{exit}}}{\sum \mathrm{CEFA_{insertion}}}\right), \text{when } \mathrm{CEFA_{insertion}} > \mathrm{CEFA_{exit}} \\ -\left[1 - \left(\frac{\sum \mathrm{CEFA_{insertion}}}{\sum \mathrm{CEFA_{exit}}}\right)\right], \text{when } \mathrm{CEFA_{insertion}} \leq \mathrm{CEFA_{exit}} \end{cases} \quad \text{Eq. 13}$$

Continuing our example, let us assume that the grower calculated a CEFS value for the block of 0.08, indicating that biomass asymmetry in the canopy caused an 8% bias in %PPF toward the insertion side of the canopy. This bias acts to offset the imbalance caused by sun tracking asymmetry, suggesting that the clusters actually received an approximately equal amount of light from either side of the canopy, despite the sun tracking bias to the exit side.

Similarly, LEFS calculations were defined by substituting LEFA for CEFA in equation 13. LEFS is expected to generally be very close to zero for most canopies,

due to the dominance of leaf contacts in PQA datasets.

Results

Canopy characterization and calibration of flux attenuation. The new metrics, when applied to the sample dataset, indicated there was an effect of shoot thinning in reducing canopy density and increasing sunlight exposure of both leaves and fruit. By traditional PQA metrics, shoot thinning decreased canopy LLN, PIC, PIL, and increased PG (Table 1.3). Using the new spatial metrics and calibrated flux metrics (Table 1.4), shoot thinning decreased canopy OLN, CEL, LEL and increased CCS, Ep1, CEFA, CEFS, and LEFA.

Table 1.3. Efficacy of shoot thinning of Vignoles expressed by traditional PQA metrics.

Treatment	LLN	PIC	PIL	PG
Control	2.53	70.78	37.19	6.31%
Shoot thinned	2.08	55.69	31.52	7.26%
Change	**-17.4%**[a]	**-21.3%**[b]	**-15.2%**[c]	**15.1%**[d]

[a] The shoot thinned canopy had a 17.4% reduction in the number of leaf layers.
[b] The shoot thinned canopy had a 21.3% decrease in the number of clusters that were partially or fully shaded.
[c] The shoot thinned canopy had a 15.2% reduction in the number of leaves that were partially or fully shaded.
[d] The shoot thinned canopy had a 15.2% increase in the number of canopy gaps.
[e] PQA, LLN, PIC, PIL, PG: point quadrat analysis, leaf layer number, percent interior clusters, percent interior leaves, percent gaps, respectively.

Table 1.4. Efficacy of shoot thinning of Vignoles expressed by new spatial metrics and calibrated flux metrics.

	Spatial Metrics				Calibrated Flux Metrics				
Treatment	**OLN**	**CEL**	**LEL**	**CCS**	**Ep1**	**CEFA**	**CEFS**	**LEFA**	**LEFS**
Control	3.23	0.98	0.47	0.006	.239	25.1%	0.115	40.0%	-0.021
Shoot thinned	2.78	0.66	0.36	0.070	.282	36.5%	0.068	45.9%	-0.018
Change	**-14.0%**[a]	**-32.5%**[b]	**-23.7%**[c]	**10.8%**[d]	**18%**[e]	**45.1%**[f]	**-47.7%**[g]	**14.8%**[h]	**-14.2%**[i]

[a] The shoot thinned canopy had a 14% reduction in occlusions layers (total contacts) versus the control.
[b] Shoot thinned canopy had a 32.5% reduction in occlusion layers between clusters and their nearest boundary.
[c] Shoot thinned canopy had a 23.7% reduction in occlusion layers between leaves and their nearest boundary.
[d] Shoot thinned canopy exhibited a 10.8% increase in cluster positioning bias, with the bias toward the insertion-side. There were 7% fewer shading layers between clusters and the insertion side of the canopy vs. the exit side.
[e] Canopy calibration showed a 18% increase in per-layer light transmittance in shoot thinned canopy vs. the control.
[f] On average, the clusters in the shoot thinned canopy received 45.1% more of the available above-canopy photon flux compared to those in the control.
[g] The shoot thinned canopy exhibited a 47.7% reduction in cluster exposure bias. Both the control and shoot thinned canopies exhibited a bias (11.5% and 6.8%, respectively) in cluster photon flux availability from the insertion side of the canopy.
[h] On average, the leaves in the shoot thinned canopy received 14.8% more of the available above-canopy photon flux compared to those in the control.
[i] The shoot thinned canopy exhibited a 14.2% reduction in leaf exposure bias. Although, both the control and shoot thinned canopies exhibited minimal (2.1% and 1.8%, respectively) bias in leaf photon flux availability from either side of the canopy.
[j] OLN, CEL, LEL, CCS, Ep1, CEFA, CEFS, LEFA, LEFS: occlusion layer number, cluster exposure layer, leaf exposure layer, canopy cluster symmetry, canopy calibration coefficient, cluster exposure flux availability, cluster exposure flux symmetry, leaf exposure flux availability, and leaf exposure flux symmetry, respectively.

Biomass exposure gradients. Cluster exposure mapping (Figure 1.1A) indicated that the clusters in the shoot thinned canopies had higher %PPF values vs. control. The exposure map indicated that largest reduction in cluster counts for shoot thinned vines occurred in the %PPF range of 15-19.9%, followed by the ranges of 25-29.9%, and 0-4.9%; while the largest increase in cluster counts for shoot thinned vines occurred in the %PPF range of 20-24.9%, followed by the ranges of 30-34.9%, 55-

58.9%, and 65-69.9%.

Similarly, LEFA values were calculated for each leaf contact in the sample data set. The resulting exposure maps (Figure 1.1B) indicated that the leaves in the shoot thinned canopies had higher %PPF values vs. control. The exposure map indicated that the largest reductions in leaf counts for shoot thinned vines occurred in the %PPF range of 50-54.9%, followed by the ranges of 15-19.9%, 60-64.9% and 25-29.9%; while the largest increase in leaf counts for shoot thinned vines occurred in the %PPF range of 55-59.9%, followed by the ranges of 65-69.9%, and 20-24.9%.

Scope of metabolic effect. Cluster exposure mapping (Fig. 1) indicated that the effects of shoot thinning on cluster exposure were concentrated in the lower %PPF ranges, with most improvements occurring for clusters originally below 30% ambient PPF. However, leaf exposure mapping (Fig. 2) revealed a concentration of efficacy in %PPF ranges above 50%. This suggests that shoot thinning treatment increased the photon flux for deeply shaded clusters more effectively than it did for deeply shaded leaves.

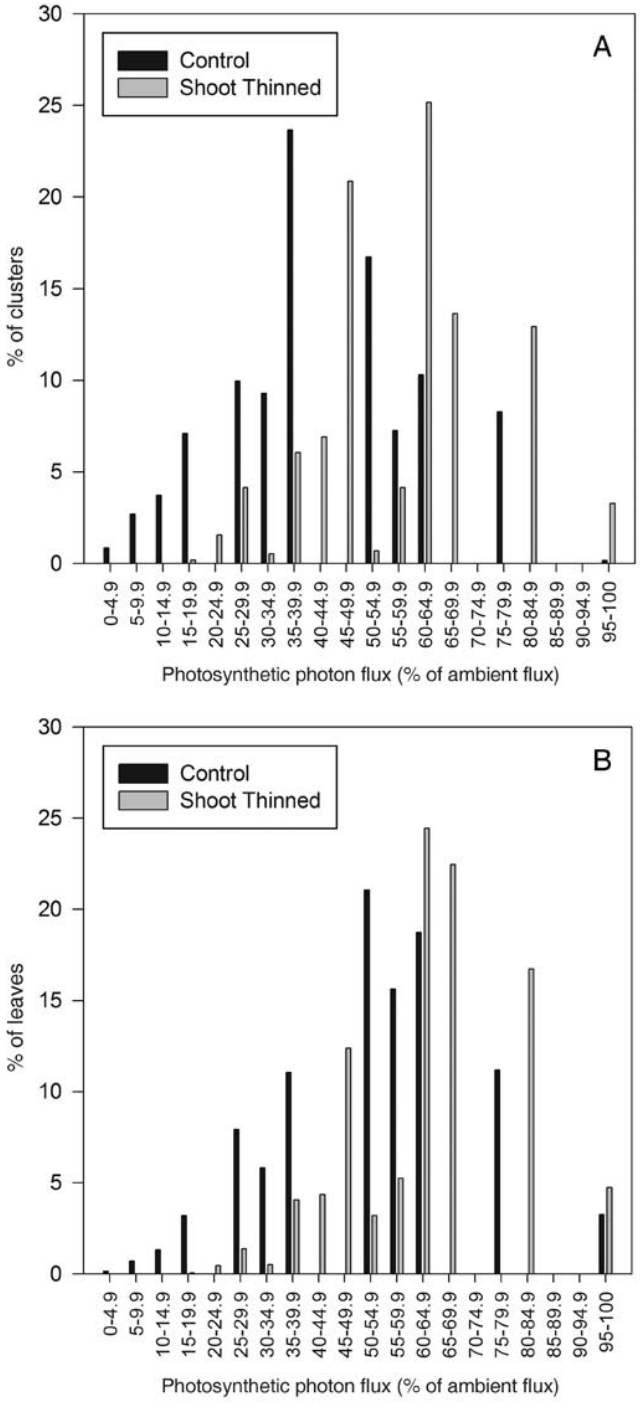

Figure 1.1. Cluster exposure map (**A**) and leaf exposure map (**B**) for sample data set. Total cluster count for control and shoot-thinned treatments was 592 and 580, respectively. Total leaf count for control and shoot-thinned treatments was 2107 and 1751, respectively.

Discussion

Improved utility. PQA's limited spatial precision has narrowed its use to diagnosing simple canopy problems and providing coarse measurements of treatment efficacy. Spatially-aware cluster and leaf exposure metrics expand PQA's usefulness by enabling the measurement of subtle differences in light environment, canopy density and biomass distribution. Canopy calibration further increases the utility of PQA by providing researchers with the tools needed to make direct quantitative comparisons among dissimilar canopies and across multiple studies. The simplicity and precision of calibrated PQA makes it an effective alternative to more time consuming coordinate-based canopy measurement techniques, and to less robust methods such as photographic sunfleck analysis.

Integration of mesoclimatic data. When temporal mesoclimatic flux data is available, it can be overlaid onto a %PPF exposure map to produce a map of absolute photon flux. These maps could be used to evaluate flux-dependent physiological responses, such as leaf light compensation point and light saturation. In this way, exposure maps could be used to estimate a variety of physiological responses, such as a canopy's potential net photosynthetic carbon production over a specific timeframe, or the development of light-sensitive metabolites.

Considerations for shoot positioned vs. non-positioned training systems. The new spatial metrics (OLN, CEL, LEL, and CCS) were intended to be equally appropriate for any type of canopy, as they do not make any assumptions regarding light attenuation – they merely improve on the spatial precision of standard PQA datasets. The metrics that rely on attenuation calibration (CEFA, LEFA, CEFS, and LEFS) are also intended to be used with any type of training system, but are probably maximally effective when applied to non-vertically positioned shoot systems, as non-vertically shoot positioned systems are more likely to have higher OLN and more

spatial distribution.

Additional research and crop management applications. The light attenuation curve for a calibrated canopy correlates with its distribution of leaf area density (Gladstone and Dokoozlian 2003). As such, the exposure maps created by the methods presented here could be used as leaf area density maps in the studying of pests and disease densities, or for the calibration of spray equipment for optimal canopy deposition. Canopy biomass symmetry and cluster exposure symmetry metrics could guide the severity and timing of alternate side leaf pulling, or other leaf density management practices. The relevance of these mapping methods need not be limited to grapevine canopies and could be applied to other row crops.

Use of model. Calculation of the new spatial metrics can be performed using traditional PQA datasets. Spatial exposure mapping, which requires a minimal number of ceptometer measurements to calibrate the canopy, adds only a few minutes of data collection time per panel. The optional trellising symmetry calculation requires only that the center of the trellis, or "wire", be recorded along with leaf and cluster contacts as a 'W' in the PQA dataset. A library of Excel spreadsheet functions that automates the data processing required to compute the new metrics is available from the corresponding author (jmm533@cornell.edu).

Conclusion

This paper demonstrated new sampling and numerical analysis methods that combined traditional PQA and photosynthetic photon flux measurements into a calibrated biomass and photon flux distribution model. These techniques, when applied to a sample dataset of control vs. shoot thinned vines, demonstrated detailed quantitative descriptions of canopy biomass distribution, light environment, and the efficacy of the viticultural treatment. In combination, the exposure maps and biomass symmetry methods should enable the synthesis of mesoclimatic photon flux data with

microclimatic indicators to further enhance the precision of efficacy correlation studies and enhance the significance of cross-study correlations. It is anticipated that these new methods may serve to guide cultural practices, and be used to predict relative fruit and wine quality from grapevine canopies at mid-way through the growing season.

LITERATURE CITED

Dokoozlian, N.K., and W.M. Kliewer. 1995a. The light environment within grapevine canopies. I. Description and seasonal changes during fruit development. Am. J. Enol. Vitic. 46:209-218.

Dokoozlian, N.K., and W.M. Kliewer. 1995b. The light environment within grapevine canopies. II. Influence of leaf area density on fruit zone light environment and some canopy assessment parameters. Am. J. Enol. Vitic. 46:219-226.

Downey, M.O., N.K. Dokoozlian, and M.P. Krstic. 2006. Cultural practice and environmental impacts on the flavonoid composition of grapes and wine: A review of recent research. Am. J. Enol. Vitic. 257-268.

Gladstone, E.A., and N.K. Dokoozlian. 2003. Influence of leaf area density and trellis/training system on the microclimate within grapevine canopies. Vitis 42:123-131.

Hashizume, K., and T. Samuta. 1999. Grape maturity and light exposure affect berry methoxypyrazine concentration. Am. J. Enol. Vitic. 50:194-198.

Lee, S., M. Seo, M. Riu, J.P. Cotta, D.E. Block, N.K. Dokoozlian, and S.E. Ebeler. 2007. Vine microclimate and norisoprenoid concentration in Cabernet sauvignon grapes and wines. Am. J. Enol. Vitic. 58:291-301.

Reynolds, A.G., and D.A. Wardle. 1989. Influence of fruit microclimate on

monoterpene levels of Gewürztraminer. Am. J. Enol. Vitic. 40:149-154.

Reynolds, A.G., D.A.Wardle, and M. Dever. 1994. Shoot density effects on Riesling grapevines: Interactions with cordon age. Am. J. Enol. Vitic. 45:435-443.

Reynolds, A.G., D.A. Wardle, and A.P. Naylor. 1996. Impact of training system, vine spacing, and basal leaf removal on Riesling. Vine performance, berry composition, canopy microclimate, and vineyard labor requirements. Am. J. Enol. Vitic. 47:63-76.

Schultz, H.R. 1995. Grape canopy structure, light microclimate and photosynthesis. I. A two-dimensional model of the spatial distribution of surface area densities and leaf ages in two canopy systems. Vitis 34:211-215.

Smart, R. E. 1985. Principles of grapevine canopy microclimate manipulation with implications for yield and quality. A review. Am. J. Enol. Vitic. 36:230-239.

Smart, R.E., and M. Robinson. 1991. Sunlight into Wine: A Handbook for winegrape canopy management. Winetitles, Underdale, Australia.

Tarara, J.M., J.C. Ferguson, G.A. Hoheisel, and J.E. Perez Pena. 2005. Asymmetrical canopy architecture due to prevailing wind direction and row orientation creates an imbalance in irradiance at the fruiting zone of grapevines. Agric. For. Meteorol. 135:144-155.

CHAPTER 2

INFLUENCE OF SHOOT THINNING AND HEDGING ON MICROCLIMATIC VARIABILITY IN VIGNOLES

Abstract: Canopy management treatments applied to control microclimatic parameters are generally assumed to improve parametric consistency, but this assumption is not often tested. To explore the effect of common canopy management on microclimatic consistency, Vignoles (Vitis sp.) vines in an established commercial vineyard were subjected to three treatments – shoot thinning (ST), hedging (H), and a combination of shoot thinning and hedging (ST-H) over a period of two years. Results indicated that occlusion layer number, a measure of biomass density, exhibits similar patterns of autocorrelation among control and treated canopies, suggesting that treatments do not reduce spatial trends. Six metrics of fruit-zone organ exposure exhibited statistically significant differences in intra-season variance, and that five of the six were a result of increases in variance, suggesting that treatments intended to influence fruit-zone organ exposure may do so with the side-effect of increased variability. When both seasons were aggregated, only two treatment-metric combinations resulted in statistically significant difference in variance, further suggesting that treatment-induced variability is not consistent from season to season.

Key words: canopy management, shoot thinning, variance equality

Introduction

Shoot thinning and hedging treatments are commonly applied with the goal of manipulating excess vine growth in a manner that improves vine performance and

fruit-zone canopy architecture. Among the many shoot thinning and hedging studies in the literature (Reynolds et al., 2005; Morris et al., 2005; Reynolds et al., 1994a; Poni et al., 2004), treatment efficacy has been largely measured in terms of responses in parameters such as yield, Brix, TA, and fruit sunlight exposure. When qualitatively interpreting results, a treatment is generally considered to successful when it achieves responses that positively correlate with contemporary models of fruit quality as in (Reynolds et al, 1994a; Reynolds et al, 1994b). From a statistical perspective, treatment response is measured a changes in mean parameter value while treatment significance is determined through a method of means separation such as analysis of variance (i.e., ANOVA).

Spatial autocorrelation in microclimatic canopy parameters has been measured and these parameters correlate with flavour compounds in winegrapes (Meyers et al., 2009). However, in reporting experimental results, parameter variability is often not quantified and if it is discussed, it is limited to a characterization naturally occurring variability (Kasimatis et al., 1975**)** or a rationalization of unexpected results as in (Reynolds et al., 2007). Since it is generally assumed that the consistent application of cultural practices will lead to reduced variability, failed statistical separation in the presence of high variability is often assumed to be the result of intrinsic vineyard variability obscuring treatment effect.

Researchers anticipate plot-scale variability, as it has been previously quantified for numerous parameters including canopy fill (Bramley and Hamilton, 2004), yield (Taylor et al., 2005), and vine water status (Acevedo-Opazo et al., 2010), so they plan for inherent variability through the use of experimental design techniques such as blocking and replication, or specialized sampling protocols that attempt to compensate for potential sources of block (Iland et al., 2004) or vine (Rankine et al., 1962) variability. Thus far, however, the hypothesis that the treatment itself could

increase parametric variability has not been tested. To test this hypothesis, shoot thinning and hedging were applied to a commercial Vignoles (*Vitis* sp.) and analyzed for its effect on the autocorrelation and variance of microclimatic parameters.

Materials and methods

Vine material. A Vignoles (*Vitis* sp.) block, approximately 25 years of age, was subjected to canopy management treatments at a commercial vineyard in Hector, NY (Finger Lakes region, east side of Seneca Lake). Vines were planted in north-south row orientation, trained to high wire umbrella, and managed according to standard viticultural practices for hybrid canopies in the Finger Lakes region. Vine spacing was 2.4 by 2.8 meters. The fruiting wire was approximately 1.8 meters above soil level. A subplot of 896 research vines was chosen from 16 consecutive rows in the block. Exterior rows and panels were excluded. Three panels were randomly chosen per row to obtain 192 research vines. The experiment consisted of 4 replications, one replication per row, of 4 treatments. The four treatments consisted of a control, shoot thinning (ST), hedging (H), and a combination of shoot thinning and hedging (ST-H). Shoot thinned vines were thinned on May 21st and May 19th, in 2007 and 2008 respectively, to a target of 20 shoots per linear canopy row meter, while the remaining (control) vines averaged 24 shoots per linear meter of canopy. All secondary and tertiary shoots were removed for ST and ST-H treatments. Hedged (H) vines were hedged on July 23th and 18th in 2007 and 2008 respectively along the face of the rows. No top-hedging was performed.

Canopy characterization. Point quadrat analysis (PQA; Smart and Robinson 1991), Enhanced point quadrat analysis (EPQA) and calibrated exposure mapping (CEM) were performed pre-veraison, after hedging, on July 23thth and July 18th in 2007 and 2008 respectively by inserting a thin metal rod into the fruiting zone along

the transverse axis of the canopy row, as described by Meyers and Vanden Heuvel (2008). A tape measure was used as a guide for insertions, which were made at 20-cm intervals along the length of the four-vine panel at the height of the fruiting wire, resulting in a total of 35 insertions per panel. A Decagon AccuPAR LP-80 photosynthetically active radiation sensor (Decagon Devices; Pullman, WA) was used to measure percent photon flux (PPF). PQA and EPQA metrics were computed for each vineyard panel using Microsoft Office Excel version 12.0.6514.5000 SP2 (Microsoft Corporation; Redmond, WA) and EPQA-CEM Tools version 1.6.2 (available on request from jmm533@cornell.edu). The following metrics were calculated: percent gaps (PG), occlusion layer number (OLN), leaf layer number (LLN), percent interior clusters (PIC), percent interior leaves (PIL), cluster exposure layer (CEL), cluster exposure flux availability (CEFA), leaf exposure layer (LEL), and leaf exposure flux availability (LEFA). As measures of 'low' and 'high' cluster exposure cluster exposure maps were computed, as described by Meyers and Vanden Heuvel (2008) to determine the percentage of clusters in each replicate with CEFA values below 0.25 (CEFA25) and above 0.75 (CEFA75) respectively.

Quantification of canopy autocorrelation. Autocorrelation in OLN was calculated in 20 cm lag distance increments along the length of each panel using the *autocorr* function from the MATLAB add-on Econometrics Toolbox version 1.1 (The Mathworks, Natick, MA, USA). Results were averaged across all panels in each treatment combination and plotted to compare the autocorrelation patterns between seasons.

Statistical Analysis. Statistical analysis was performed via SAS version 9.1.3, service pack 4 (SAS; Cary, NC) for treatment mean, standard deviation, least-squares mean separation, pairwise least-significant-difference (LSD) *t* tests, Levene tests (Levene 1960) of variance equality, and Brown-Forsythe (BF; Brown and Forsythe

1974) tests for pairwise (i.e. control vs. treatment) variance equality. Significance was reported, for all tests, only when *p*-values were less than 0.05. Variability of each parameter was quantified by computing relative standard deviation (RSD) for each treatment. The components of RSD (mean and standard deviation) and RSD value (100 * mean / standard deviation) were computed via Microsoft Office Excel version 12.0.6514.5000 SP2 (Microsoft Corporation; Redmond, WA).

Results

Autocorrelation of canopy biomass. Spatial autocorrelation of OLN was present in all treatments and varied with lag distance (Figure 2.1). All autocorrelation plots revealed a visible sinusoidal hole-effect pattern, modulating between positive and negative values.

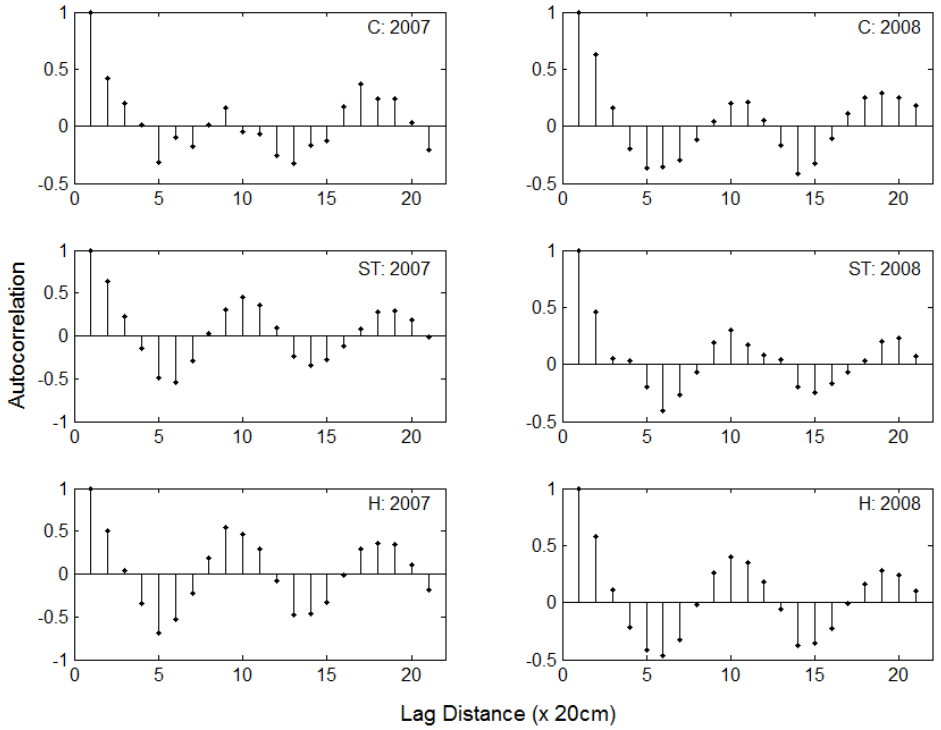

Figure 2.1. Average spatial autocorrelation (range -1 to 1) of Occlusion Layer Number (OLN). By definition, a lag distance of zero has an autocorrelation value of '1'. The sinusoidal "hole-effect" pattern is visually apparent in all plots (C = control, ST = shoot-thinned, H = hedged).

Microclimatic response. In 2007, the ST treatment resulted in a statistically significant response in all canopy metrics except PG (all canopy responses shown in Table 2.1). 2007 ST reduced canopy density (OLN = 2.67 vs. control of 3.44; LLN = 2.00 vs. control of 2.71) and increased fruit-zone organ exposure (PIC = 52.2% vs. control of 73.7%; PIL = 27.3% vs. control of 37.5%; CEL = 0.63 vs. control of 0.96; LEL = 0.30 vs. control of 0.46; CEFA = 0.54 vs. control of 0.40; LEFA = 0.61 vs. control of 0.51; CEFA75 = 14% vs. control of 2%) while specifically reducing the percentage of low-exposure clusters (CEFA25 = 7% vs. control of 25%).

2007 H resulted in only a single significant response (PG = 9.29% vs. control of 3.33%), while 2007 ST-H resulted in statistically significant reductions of measures of canopy density (OLN = vs. control of; LLN = vs. control of), and increases in most measures of fruit-zone organ exposure (PIC = 55.6% vs. control of 73.7%; CEL = 0.65 vs. control of 0.96; CEFA = 0.57 vs. control of 0.40; CEFA25 = 5% vs. control of 25%; CEFA75 = 16% vs. control of 2%). Average 2007 yields on a panel-basis were C = 31.2 (+/- 19.7); ST = 24.1 (+/- 15.1); H = 23.9 (+/- 16.4); ST-H = 26.0 (+/- 16.3).

In contrast, 2008 ST (Table 2.1) resulted in no statistically significant canopy responses, while H reducing measures of canopy density (PG = 16.3% vs. control of 8.59%; OLN = 2.16 vs. control of 2.84; LLN = 1.70 vs. control of 2.27) and increasing measures of fruit-zone organ exposure (PIC = 35.7% vs. control of 53.5%; PIL = 23.1% vs. control of 35.1%; CEL = 0.25 vs. control of 0.70; LEL = 0.26 vs. control of 0.43; LEFA = 0.50 vs. control of 0.45). Average 2008 yields on a pounds-per-panel-basis were C = 40.5 (+/-7.0); ST = 54.0 (+/- 69.2); H = 29.6 (+/- 11.9); ST-H = 30.9 (+/- 15.8).

Table 2.1. Canopy architecture metrics.

Year	Treatment	PG	OLN	LLN	PIC	PIL	CEL	CEFA	LEL	LEFA	% of clusters w/CEFA < 0.25	% of clusters w/CEFA > 0.75
2007	C	3.33 (5.14) b	3.44 (0.56) a	2.71 (0.39) a	73.7 (10.9) a	37.5 (6.9) a	0.96 (0.25) a	0.40 (0.06) b	0.46 (0.12) a	0.51 (0.04) b	25 (10) a	2 (3) a
	ST	6.90 (5.09) ns	2.67 (0.56) b **	2.00 (0.45) b ***	52.2 (20.9) b ***	27.3 (7.6) b **	0.63 (0.30) b **	0.54 (0.07) a ****	0.30 (0.09) b **	0.61 (0.05) a ****	7 (7) b ***	14 (11) b **
	H	9.29 (9.83) a *	3.02 (0.82) ns	2.34 (0.71) ns	66.7 (17.3)	33.4 (10.0) ns	0.91 (0.51) ns	0.41 (0.11) ns	0.42 (0.19) ns	0.52 (0.08) ns	23 (23) ns	5 (7) ns
	ST-H	7.62 (5.49) ns	2.88 (0.30) b *	2.17 (0.30) b **	55.6 (10.8) b ***	33.9 (5.3) ns	0.65 (0.15) b *	0.57 (0.07) a ****	0.39 (0.07) ns	0.62 (0.06) a ****	5 (6) b ***	16 (11) ns
2008	C	8.59 (7.38) b	2.84 (0.63) a	2.27 (0.56) a	53.5 (14.2) a	35.1 (9.1) a	0.70 (0.26) a	0.40 (0.09)	0.43 (0.17) a	0.45 (0.05) b	38 (16)	53 (14)
	ST	8.77 (6.32) ns	2.64 (0.65) ns	2.15 (0.59) ns	53.7 (17.8) ns	29.8 (9.4) ns	0.70 (0.31) ns	0.13 (0.21) ns	0.34 (0.15) ns	0.48 (0.06) ns	41 (19) ns	5 (7) ns
	H	16.3 (11.2) a *	2.16 (0.78) b **	1.70 (0.65) b **	35.7 (17.6) b **	23.1 (11.4) b ***	0.25 (0.18) b **	0.46 (0.15) ns	0.26 (0.16) b ***	0.50 (0.08) a *	30 (19) ns	13 (19) ns
	ST-H	10.1 (8.10) ns	2.51 (0.48) ns	1.98 (0.40) ns	56.8 (10.3) ns	28.3 (7.9) b *	0.51 (0.12) ns	0.43 (0.08) ns	0.32 (0.11) b *	0.49 (0.06) ns	32 (16) ns	6 (6) b ***

Parenthesized values are standards deviations (calculated on a per-panel basis)
* = $p < 0.05$; ** = $p < 0.01$; *** = $p \leq 0.001$; **** = $p \leq 0.0001$. Means separations apply only to same-season data

Treatment effect on canopy architecture variability. Variability in canopy architecture parameters, as shown by the RSD values in Table 2.2, varied across treatments and seasons. Levene and BF tests revealed instances of statistically significant differences in treatment parameter variability vs. control. In 2007 the ST treatment influenced variability in PIC and CEFA75, while increasing RSD to 40.1% vs. control of 14.8% and decreasing RSD in CEFA75 (80.4% vs. control of 137.6%). The 2007 H treatment significantly influenced variability in CEFA, LEFA, CEFA25, and CEFA75 vs. control. Compared to control, RSDs increased in CEFA (27.4% vs. 15.2%), LEFA (15.7% vs. 8.3%) and CEFA25 (98.3% vs 41.9%); while in CEFA75, RSD was equal vs. control (137.6) despite the statistically significant difference in variance. 2007 ST-H reduced RSD of CEFA75 (68.5%) vs. control (137.6%). 2008

data indicated that only one treatment-parameter combination resulted in significantly different variance, with the H treatment reducing the RSD of PG (68.6%) vs. control (85.9%).

Table 2.2. Relative standard deviation and variance equality tests of canopy metrics

Treatment	Year	PG	OLN	LLN	PIC	PIL	CEL	CEFA	LEL	LEFA	% of clusters w/CEFA ≤ 0.25	% of clusters w/CEFA > 0.75
2007	C	154.3	16.2	14.5	14.8	18.4	26.5	15.2	26.9	8.3	41.9	137.6
	ST	73.7	21.1	22.6	*40.1* *	27.8	47.9	13.6	31.2	8.2	101.1	*80.4* †
	H	105.9	27.1	30.3	26.0	29.9	56.2	*27.4* *†	46.1	*15.7* *†	*98.3* *†	*137.6* *
	ST-H	72.1	10.5	14.0	19.3	15.5	23.5	12.6	17.1	9.2	124.0	*68.5* *†
2008	C	85.9	22.3	24.8	26.5	25.9	37.4	22.4	38.6	10.0	42.8	96.0
	ST	72.1	24.5	27.3	33.1	31.7	45.2	26.2	43.3	12.2	45.6	135.1
	H	*68.6* †	36.1	38.1	49.3	49.3	65.0	32.4	60.2	15.3	63.1	150.6
	ST-H	80.6	19.2	20.4	22.0	28.0	24.3	17.6	33.5	11.7	51.4	101.2
Combined	C	113.6	21.0	21.1	25.3	22.0	34.5	18.8	32.4	10.4	47.3	129.2
	ST	72.6	22.3	25.0	35.9	29.6	45.7	*25.3* *	38.2	*15.3* *†	*92.7* †	107.1
	H	*85.2* *†	34.6	36.6	*45.5* *†	*41.5* *	70.8	*30.4* *†	56.0	*15.4* *†	78.1	166.8
	ST-H	77.9	16.2	17.5	22.0	23.0	*26.1* *†	20.2	26.5	*15.5* *†	100.4	92.9

† = Brown-Forsythe test for variance equality rejects null hypothesis (that variances are equal) with $p < 0.05$.
* = Levene test for variance equality rejects null hypothesis (that variances are equal) with $p \leq 0.05$.

Discussion

Increased fruit-zone exposure variability. In metrics of fruit-zone organ exposure (i.e. PIC, PIL, CEL, LEL, CEFA, LEFA, CEFA25, and CEFA75), five of the six reported statistically significant differences in intra-season variance were a result of increases in variance, suggesting that treatments intended to influence fruit-zone organ exposure may do so with the side-effect of increased variability – despite their consistent application. When both seasons were aggregated, only two treatment-metric combinations resulted in statistically significant difference in variance (one increased RSD while one decreased), further suggesting that treatment-induced variability is not consistent from season to season.

Implications for precision canopy management. The concept of *precision*

viticulture applies to the variable application of cultural inputs in response to observed variability in vineyard-scale parameters (Bramley and Hamilton 2004), such as water status or canopy photosynthetic activity, with the goal of improving overall vineyard consistency. Considering the presence of spatial autocorrelation of microclimatic parameters, and the sensitivity some of odor active compounds to small differences in canopy architecture (Meyers et al., 2009), growers should consider the possibility that a consistently-applied canopy treatment, designed to reduce vineyard-scale consistency, may lead to a decrease in microclimatic consistency when applied without regard to small scale spatial patterns.

This consideration could be particularly important when trying to minimize an undesirable aroma compound that is both highly odor-active and susceptible to small differences in microclimatic parameters such as 1,1,6-trimethyl-1,2-dihydronapthalene (TDN; Kwasniewski et al., 2010; Meyers et al., 2009). Furthermore, TDN has been shown to respond to cluster exposure only at levels above 20% of ambient light (Gerdes et al., 2002; Meyers et al., 2010 unpublished data). Considering these model parameters, managing a Riesling vineyard to a mean cluster exposure target of 20% would be a reasonable approach to minimizing TDN. However, as variability in cluster exposure increases, so will the number of clusters receiving more than the 20% threshold of dose response. Although increased variance will also increase the number of clusters receiving less than 20%, the outliers do not cancel each out (in terms of TDN response) because all clusters receiving less than 20% of ambient sunlight are expected to produce statistically equivalent TDN concentrations. Thus, in this scenario, higher variability leads to higher TDN. In these instances, it may be best to quantify small-scale variability (i.e. at the panel and/or vine level) to determine an optimal vineyard inputs that.

Conclusions

The presence of biomass spatial autocorrelation in all treatments suggests that spatially uniform application of canopy management treatments may not lead to reduction in variability. Moreover, the application of canopy management treatments intended to control fruit quality can lead to increased variability of microclimatic parameters which, in some cases, could lead to unintended degradation in fruit quality.

LITERATURE CITED

Brown, M.B. and A.B. Forsythe. 1974. Robust tests for equality of variances. Journal of the American Statistical Association, 69: 364-367.

Gerdes, S.M., P. Winterhalter, and S.Ebeler. 2002. Effect of sunlight exposure on norisoprenoid formation in white Riesling grapes. Carotenoid-Derived Aroma Compounds. Chapter 19, pp 262–272.

Kwasniewski, M.T., J.E. Vanden Heuvel, B.S. Pan, and G.L. Sacks. 2010. Timing of cluster light Environment Manipulation during Grape Development Affects C13 Norisoprenoid and carotenoid concentrations in Riesling. J. Agric. Food Chem. In press.

Levene, H. 1960. Robust Tests for Equality of Variances, in Contributions to Probability and Statistics, ed. I. Olkin, Palo Alto, CA: Stanford Univ. Press.

Meyers, J.M., G.L. Sacks, H.M. van Es, and J.E. Vanden Heuvel. 2010. Improving efficiency of research and vineyard operations via spatially-explicit sampling protocols. 2010 American Society of Enology and Viticulture, National Meeting. Seattle, WA. In press.

Meyers, J.M. and J.E. Vanden Heuvel. 2009. Spatial correlation in vine biomass density suggests need for new design and sampling protocols. Am. J. Enol. Vitic. 60(4): 553A.

Meyers, J.M., G.L. Sacks, and J.E. Vanden Heuvel. 2009. Naturally occurring spatial variability in canopy biomass impacts flavor and aroma compounds in riesling. Am. J. Enol. Vitic. 59(4): 394A-395A.

Meyers, J.M., and J.E. Vanden Heuvel. 2008. Enhancing the precision and spatial acuity of point quadrat analyses via calibrated exposure mapping. Am. J. Enol. Vitic. 59:424-431.

Morris, J.R., G.L. Main, and O.L. Oswald. 2004. Flower cluster and shoot thinning for crop control in French-American hybrid grapes. Am. J. Enol. Vitic. 55:423-426.

Poni, S., F. Bernizzoni, P. Presutto, and B. Rebucci. 2004. Performance of Croatina under short-cane mechanical hedging: A successful case of adaptation. Am. J. Enol. Vitic. 55:379-388.

Reynolds, A.G., I.V. Senchuk, C. van der Reest, and C. de Savigny. 2007. Use of GPS and GIS for elucidation of the basis for terroir: Spatial variation in an Ontario Riesling vineyard. Am. J. Enol. Vitic. 58:145-162.

Reynolds, A.G., T. Molek, and C. De Savigny. 2005. Timing of shoot thinning in vitis vinifera: impacts on yield and fruit composition variables. Am. J. Enol. Vitic. 56: 343 – 356.

Reynolds, A.G., C.G. Edwards, D.A. Wardle, D.R. Webster, and M. Dever. 1994a. Shoot density affects Riesling grapevines: I. Vine performance. J. Am. Soc. Hortic.

Sci. 119:874-880.

Reynolds, A.G., C.G. Edwards, D.A. Wardle, D.R. Webster, and M. Dever. 1994b. Shoot density affects Riesling grapevines: II. Wine composition and sensory response. J. Am. Soc. Hortic. Sci. 119:881-892.

Reynolds, A.G., R.M. Pool, and L.R. Mattick. 1986. Effect of shoot density and crop control on growth, yield, fruit composition, and wine quality of Seyval blanc. J. Am. Soc. Hortic. Sci. 111:55-63.

Smart, R.E., and M. Robinson. 1991. Sunlight into Wine: A Handbook for winegrape canopy management. Winetitles, Underdale, Australia.

Tamura, R.N., L.A. Nelson and G.C. Naderman. 1988. An investigation on the validity and usefulness of trend analysis for field plot design, Agron. J. 80:712–718.

CHAPTER 3

MAXIMIZING OPERATIONAL EFFICIENCY VIA DYNAMIC SPATIALLY-EXPLICIT OPTIMIZATION

Abstract: Environmental parameters within vineyards are spatially correlated, impacting the economic efficiency of cultural practices and accuracy of viticultural studies that utilize random sampling. This study aimed to test the performance of non-random sampling protocols that account for spatial correlation ("spatially-explicit protocols") in reducing sampling requirements versus random sampling and decreasing the negative impacts of spatial imbalance.

Canopy microclimate data was collected across multiple sites/seasons/training systems. Autocorrelation was found in all systems, with a periodicity generally corresponding to vine spacing. Three spatially-explicit sampling models were developed to balance minimal sample sizes against maximal fit of sample fruit exposure parameters to population parameters. A globally optimized explicit sampling (GOES) model, which performed multivariate optimization to determine best-case sampling locations, reduced fruit cluster sample size requirements vs. random sampling by up to 60%. Two univariate spatially-weighted template sampling (STS) models, derived from GOES solutions but easier to implement, reduced sampling requirements up to 24% when based on probabilistic panel weighting (PW), and up to 21% when preferentially selecting specific locations within canopy architecture (AW).

GOES, PW STS, and AW STS each reduced required sample size vs. random sampling. Comparative analyses suggested that optimal sampling strategies should simultaneously account for spatial variability at multiple scales. This study, one of the first agricultural studies on the use of spatially-explicit sampling protocols,

demonstrates that dynamically optimized sampling can decrease sample sizes required by researchers and/or wineries and reduce the negative impact of spatial imbalance within vineyards.

Key words: autocorrelation , canopy management, cluster exposure, heuristic algorithms, sampling strategies

Introduction

Viticulturalists collect quantitative data on vine characteristics and fruit composition to understand and guide cultural practices. However, vineyards are heterogeneous and many key viticultural parameters vary significantly throughout a site. For example, soluble solids in single Thompson Seedless berries within the same vineyard are reported to have a standard deviation of 1.7 – 3.0 degrees Brix (Kasimatis et al., 1975). Similarly, vine-level spatial autocorrelation in microclimatic canopy parameters has been measured by enhanced point quadrat analysis (EPQA; Meyers and Vanden Heuvel, 2008), and these parameters correlate with flavour compounds in winegrapes (Meyers et al., 2009). Block-level spatial patterns in vineyards have been identified and quantified for a variety of parameters, including canopy fill (Bramley and Hamilton, 2004), yield (Taylor et al., 2005), and vine water status (Acevedo-Opazo et al., 2010).

To address inherent variability within a block or vineyard, viticulturalists typically pool together multiple berries or clusters to improve accuracy, and test samples in replicate to evaluate the precision of their measurements and facilitate statistical comparisons. Both commercial growers and researchers aim to minimize the number and size of field samples to reduce labour and material costs while still achieving acceptable accuracy and precision. Many sampling protocols have been

suggested for collecting fruit from vineyards, with the majority of approaches involving random selection of clusters from either the whole vineyard or a vineyard sub-section. Some sampling protocols involve the use of generalized spatial patterns to, for example, ensure that fruit is sampled from all regions of an individual vine (Rankine et al., 1962), or balanced across sides of a row (Iland et al., 2004).

From a statistical perspective, the ideal protocol should result in a *representative sample* of the population, such that parameters are sampled with a distribution similar to that of the population. The justification for random sampling is that variables contributing to the variance of a population are expected to be mutually independent with respect to their location in time and space, i.e., *independent and identically-distributed (i.i.d.) random variables*. Under these circumstances, any arbitrary set of sampled field measurements is equivalent to any other set (of equal size) in its ability to estimate population parameters, hence the standard use of random sampling in viticultural experiments.

When random variables in a system are *i.i.d.*, that system is said to be a *stationary process* with respect to the measured variables. The term *stationarity* is used to describe the stationary nature of statistical parameters within a system – such as the mean and variance. If the mean in a system is independent of both time and space, the system is said to exhibit first order stationarity. Similarly, second order stationarity is said to exist when the variance of a system does not vary as a function of location. Because the practice of random sampling assumes *i.i.d.*, its accuracy and efficiency is a function of the first and second order stationarity of the system in which it is employed.

The realization that random variables are not *i.i.d.* for most agricultural plots (Student, 1938; Jefferys, 1939) has led to the introduction of blocking and replication to compensate for potential spatial patterns. In modern agricultural experiments, this

compensation often takes the form of randomized complete block designs (RCBD) and their variants. For the most part, these techniques are applied to experimental designs without attempting to gain prior knowledge of existing field patterns (van Es et al. 2007), despite the demonstration that direct compensation for known spatial trends can improve precision in hypothesis testing (Kirk et al., 1980; Tamura et al., 1988). In viticultural literature, some authors have suggested using systematic approaches to sample berries from all parts of the cluster as opposed to randomly selecting berries (Roessler and Amerine, 1958; Rankine et al., 1962, Iland et al., 2004) to compensate for variability in ripeness, but to our knowledge, vineyard sampling protocols that account for known spatial heterogeneity within a site (i.e., "spatially-explicit") have not been explored. An alternative to RCBD, the spatially-balanced complete block (SBCB) design, was developed to assist researchers in minimizing the effects of unknown block-level spatial trends (van Es et al. 2007) through the use of static block-layout templates. Because they are designed to maintain spatial balance among treatments in factorial experiments, SBCB designs are superior to RCBD in their ability to protect against the adverse effects of unknown field trends such as those reported in vineyards (Bramley and Hamilton, 2004; Taylor et al., 2005; Meyers and Vanden Heuvel, 2009; Acevedo-Opazo et al., 2010). The concept of spatially explicit design could be extended to field sampling practices to maximize the fit of a sample distribution to population statistics, such that a smaller spatially-explicit sample should achieve the same accuracy and precision as a larger random sample.

For our initial investigations of spatially-explicit sampling protocols we used measurements of canopy microclimate as the parameters of interest, as canopy microclimate is widely reported to influence many aspects of both grape and wine composition. Using natural variation in fruit cluster sunlight exposure in Riesling (*Vitis vinifera* L.) and Vignoles (*Vitis* sp.) populations from the Finger Lakes region of

New York State, we quantified autocorrelation in key microclimatic canopy parameters. We then determined the maximum potential benefit in reducing sample size using spatially-explicit globally optimized (i.e., cluster-specific) sampling methods versus randomized sampling methods. Finally, in the interest of convenient application, we considered the use of univariate "sampling template" strategies where clusters were preferentially sampled from specific regions within each panel, or from particular panels within the vineyard and used these findings to evaluate the impact of vine spacing and training systems on optimal sampling strategies.

Materials and Methods

Vine material. Three commercial New York vineyards (Finger Lakes region, east side of Seneca Lake) designated as sites 'A', 'B', and 'C' were used for this study. At site A, 66 Riesling vines (22 three-vine panels) trained to two-tier flatbow (as described by Reynolds and Vanden Heuvel, 2009) with vertical shoot positioning (VSP) were selected for consistency (i.e., no missing vines or obviously young replants) from a subplot of 6 rows. At site B, 72 Scott Henry trained (as described by Reynolds and Vanden Heuvel, 2009) Riesling vines (18 four-vine panels) were selected for consistency from a subplot of 7 rows. At site C, 96 Vignoles (*Vitis* sp.) vines (24 four-vine panels) trained to high-wire umbrella kniffen (as described by Reynolds and Vanden Heuvel, 2009) were selected at random from a subplot of 16 rows. Vines at all three sites were planted in north-south row orientation and managed according to standard regional viticultural practices. Vine spacing was 280 cm (row) x 200 cm (vine), 280 cm x 200 cm, and 280 by 180 cm for sites A, B, and C respectively. Data were collected at each site for two consecutive seasons (2008 and 2009 for sites A and B; 2007 and 2008 for site C).

Canopy density and cluster exposure characterization. EPQA and

calibrated exposure mapping (CEM) (Meyers and Vanden Heuvel, 2008) were performed at the onset of veraison (18th of July 2007 and 15th of July 2008 for Vignoles; 25th of August 2008 and 20th of August 2009 for Riesling). A tape measure was used as a guide for insertions, which were made at 20 cm intervals along the length of the panels at the height of the fruiting wire, resulting in 30, 39, and 35 insertions per panel at sites A, B, and C respectively. A Decagon AccuPAR LP-80 photosynthetically active radiation sensor (Decagon Devices, Pullman, WA, USA) was used to measure percent photon flux (PPF) values used in canopy calibration. The EPQA metrics occlusion layer number (OLN), cluster exposure layer (CEL), and cluster exposure flux availability (CEFA) were calculated as measures of canopy biomass density, un-calibrated cluster exposure, and calibrated cluster exposure, respectively using Microsoft Office Excel version 12.0.6514.5000 SP2 (Microsoft Corporation, Redmond, WA, USA) and EPQA-CEM Tools version 1.6.2 (available on request from jmm533@cornell.edu). A separate dataset was computed and maintained for each site.

Quantification of canopy autocorrelation. Autocorrelation in OLN, CEL, and CEFA was calculated in 20 cm lag distance increments along the length of each panel using the *autocorr* function from the MATLAB add-on Econometrics Toolbox version 1.1 (The Mathworks, Natick, MA, USA). Results were averaged across all panels in each site-year combination and plotted to compare the autocorrelation patterns between seasons and among the three tested EPQA metrics. To quantify potential repetitive spatial patterns in canopy architecture parameters, Fourier series were computed for each EPQA metric, as a function of distance along canopy row. Fourier signal periods were computed using MATLAB's discrete Fourier transform function, *fft*, and additionally processed via custom software.

Simulated sampling using real field data. A fruit cluster contact database for

each site-year combination was created by exporting the calculated EPQA-CEM values as measured at veraison (i.e., OLN, CEL, and CEFA) along with location information (vineyard row number, panel number, and EPQA insertion position) to a text file containing a unique data record for each cluster. The six resulting cluster inventories (three sites in each of two years) contained 706 and 819 clusters from 66 vines at site A in years 2008 and 2009 respectively; 1178 and 967 clusters from 72 vines at site B in years 2008 and 2009 respectively; and 591 and 490 clusters from 96 vines at site C in years 2007 and 2008 respectively. These databases were imported into custom-written MATLAB software (Version 7.10.0.499, The Mathworks, Natick, MA) designed to perform spatial analysis and to simulate both random sampling and spatially-explicit methods described below. The cluster inventory for each site assumed the role of that site's experimental population for the remainder of the experiment.

Determination of arbitrary sample fitness. A numerical measure of sample fitness, i.e., the similarity of any given random or spatially-explicit sample to its parent population parameters, was computed as follows: 1) Cluster exposure maps, defined as a set of CEFA values binned in 1% increments, were calculated to establish a histogram representing the discrete probability density of population cluster exposure for each site's cluster inventory, $P(CEFA_{Pop})$, and formatted as a vector of 100 histogram bins. 2) A similar vector representing the CEFA probability density of a particular sample, $P(CEFA_{Sample})$, was computed for every sample generated during a simulation. 3) Sample fitness was determined by subtracting the $P(CEFA_{Sample})$ vector from the $P(CEFA_{Pop})$ vector and computing Euclidean length of the resulting vector.

Determination of random sample fitness. A baseline model of random sample fitness was established through simulation for the purpose of later comparison with spatially-explicit sample fitness scores. The baseline was determined by

computing the fitness scores of simulated random samples ranging in size from 1% to 100% of the population equally spaced in 1% increments. To account for variation in results, the simulation was repeated in 30 trials and the final fitness score for each sample size was determined as the averaged score across all trials.

Determination of globally optimal samples. Maximally fit samples were calculated to establish the best-case of spatially-explicit sampling performance. These *globally optimized explicit samples* (GOES) were computed by searching for the maximally fit combination of clusters (i.e., the sample with the best sample fitness score) from the known population while constrained only by a target sample size (e.g., 5% of population) and without regard for balancing the sample among individual vines or panels.

Due to the combinatorial complexity of the problem space (e.g., exploring every sampling combination of 80 clusters in a population of 800 would require computing the sample fitness value of over 10^{100} sampling combinations), heuristic methods were used to identify the optimal sampling locations for each sample size. Two heuristic optimization methods, Tabu Search (TS; Glover 1990) and Genetic Algorithm (GA; Holland 1975) were implemented to perform a minimization of sample fitness score (with 0 as a perfect score) while searching the global sample space for samples of the specified size. A preliminary comparison of algorithm performance, using a subset of the experimental data, indicated that TS and GA optimizations converged on functionally equivalent solutions, but that TS found its minimum for our fitness function in about 10% of the computing time required by GA. Thus, TS was chosen for use in this experiment and the complete set of simulation trials, which analysed approximately 1.2 billion sample combinations, was computed in <48 hours processing time using a personal workstation. The specific configuration included a multi-core CPU running at 2.5GHz and enough physical

memory (i.e., 8 gigabytes) to host the algorithms without the need to access secondary storage.

Our custom simulation software was used to identify the optimal GOES solutions for samples ranging in size from 1% to 100% of the population equally spaced in 1% increments. The simulation was repeated in 30 trials and the final fitness score for each sample size was determined as the averaged score across all trials. Cluster sampling location data from the 30 trials was analysed to determine the probability of each cluster being included in the optimal sampling solution. Results were plotted, one plot for each site-year combination, to illustrate the spatial patterns and their relationship to sample size.

Spatially-explicit sampling models. In the interest of developing simple field methods and illuminating the relationships between block variability, canopy structure, and optimal sampling solutions, two strategies for *spatially-weighted template sampling* (STS) were developed which employed a form of pseudo-random sampling that concentrated sampling frequencies within specific blocks or panel locations in quantities proportionate with the globally optimized probability densities. For each site-year combination, GOES solutions were analysed to determine the inter-panel and intra-panel probability densities of optimal cluster sampling locations. These densities were used to define two types of weighted sampling templates: a panel-weighted (PW) template which determined the number of clusters to be harvested from each panel within the block; and a canopy architecture-weighted (AW) template that assigned a weighted number of clusters to each 20cm increment along the length of a panel. Figure 3.1 illustrates an example of each sampling method.

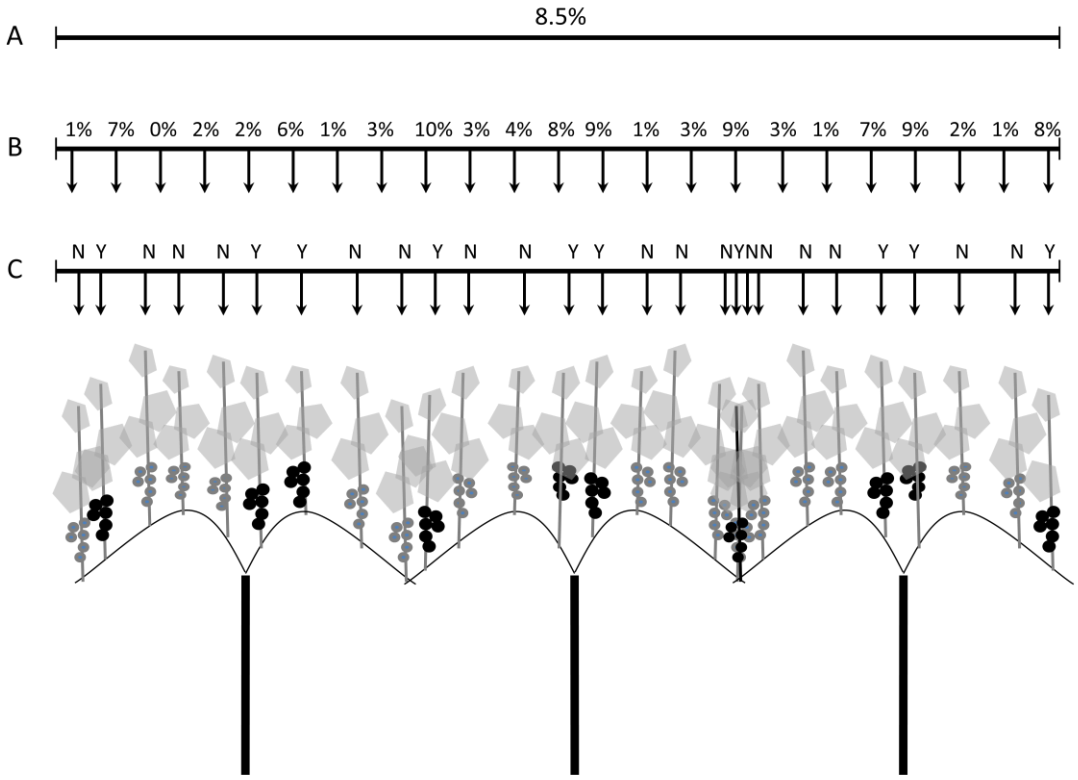

Figure 3.1. Example of a panel-weighted (A), architecture-weighted (B), and globally optimized (C) sampling template generated from EPQA dataset. The panel-weighted template indicates what percentage of the overall vineyard sample should be collected from this panel (i.e., 8.5% of the total sample – other panels will have different weights and all weights add up to 100%). The architecture-weighted sampling template indicates what percentage of the overall vineyard sample should be collected from this location along the length of each panel (applied consistently to each panel). The locations are based on 20cm increments and the weights add up to 100% for each panel. The globally optimized template indicates precisely which clusters should be sampled from each panel (Y = sample, N = do not sample). Each panel has a unique template.

Efficiency of GOES and STS vs. random sampling. Fitness values vs. sample size (1% to 100% of population) were determined for random, GOES, and STS sampling protocols as described in previous paragraphs. For each site-year combination, the resulting sample size vs. fitness scores were fitted as a series of piecewise cubic polynomials, as determined by the MATLAB *spline* function. The

fitted curves were then used to compute random-sample-equivalent sample sizes for each GOES and STS sample. Figure 3.2 illustrates the method of using the fitted curves to convert from a random sample size to an optimized sample size. Differences in sample size were plotted for each site-year combination.

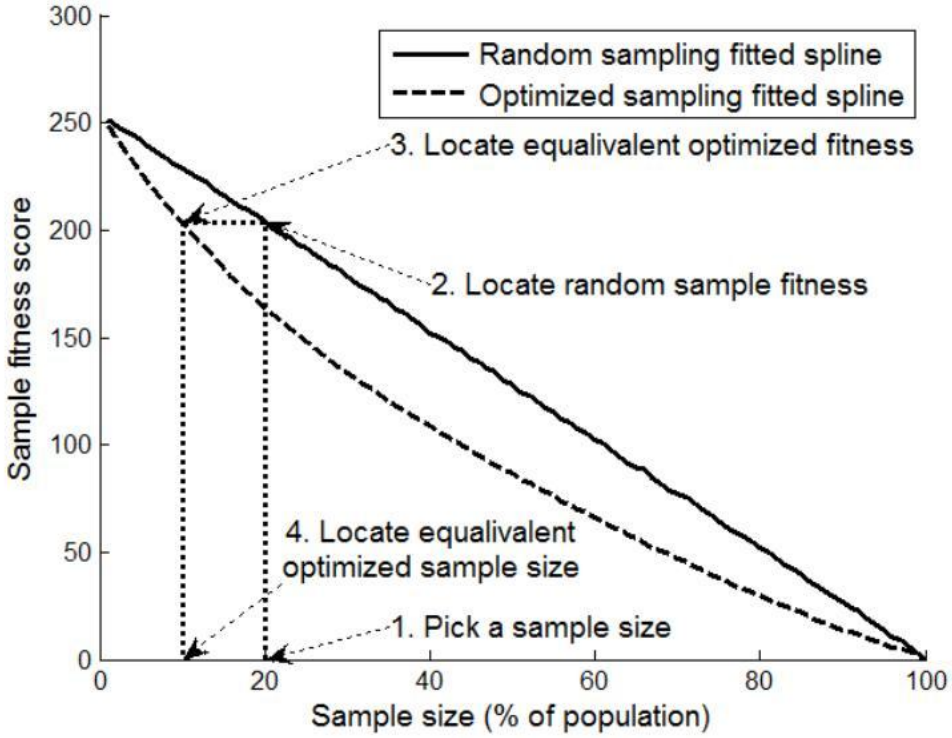

Figure 3.2. Illustration of the method used to interconvert sample size equivalents. A piecewise cubic spline was fitted to plots of fitness score vs. random sampling and fitness score vs. optimized sampling. Equivalent sample sizes are determined by locating the point on each curve where the fitness values are equal. Fitness score represents the 2-norm of the difference between population and sample discrete probability densities of the target vineyard parameters.

Results

Quantification of canopy autocorrelation. Spatial autocorrelation was present in all canopies, for all measured EPQA metrics, and varied with lag distance

(Table 3.1). Aggregated by EPQA metric, absolute mean autocorrelation for OLN, CEL, and CEFA were 0.22 (+/- 0.09), 0.13 (+/- 0.02), and 0.12 (+/- 0.02) respectively. Aggregated by training system, absolute mean autocorrelation for U, SH, and 2TFB were 0.17 (+/- 0.10), 0.16 (+/- 0.09), and 0.14 (+/- 0.02) respectively. Autocorrelation, expressed as aggregated absolute mean, varied among reported EPQA metrics with values of 0.22 (+/- 0.09), 0.13 (+/- 0.02) and 0.12 (+/- 0.02) for OLN, CEL, and CEFA respectively.

Periodic spatial structure. Most autocorrelation plots revealed a visible sinusoidal hole-effect pattern, modulating between positive and negative values (illustrated in Figure 3.3 for site C; sites A and B not shown). Fourier analysis of the underlying EPQA metrics at site A determined that the primary OLN and CEL value cycles occurred at a period of 170 and 190 canopy row centimetres (i.e., 8.5 and 9 lags) for 2007 and 2008 respectively – a distance within 10 cm of the vine spacing at that site. Primary CEFA value cycles occurred at 170 cm in 2007 and 84 cm (approximately ½ of the vine spacing) in 2008. The primary and secondary signal periods for site C are annotated on Figure 3.3, and the complete Fourier dataset is presented in Table 3.1.

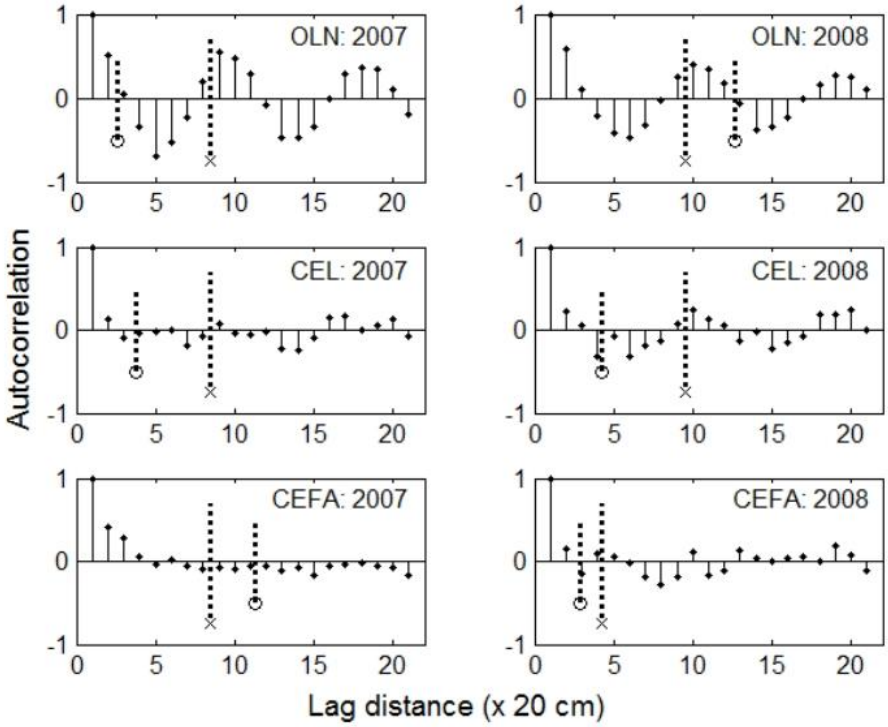

Figure 3.3. Average spatial autocorrelation (range -1 to 1) of EPQA metrics in Umbrella trained Vignoles vines (site C). By definition, a lag distance of zero has an autocorrelation value of '1'. The sinusoidal "hole-effect" pattern, attributed to the repetitive spatial structure of the canopy row along its longitudinal axis, is most evident in occlusion layer number (OLN) which is a measure of canopy biomass. The dashed line located by the 'x' indicates the most prominent signal period as determined by Fourier analysis of the underlying EPQA metrics. The dashed line located by the 'o' indicates the signal period of next highest power. Vine spacing in the field is 180 cm (9 lags). CEL = Cluster Exposure Layer, CEFA = Cluster Exposure Flux Availability.

Table 3.1. Summary statistics for canopy autocorrelation and Fourier analysis of signal periods. Bolded signal values are within 10 cm of the vine spacing (i.e. 190 cm). Italicized values represents periods consistent with double or half vine spacing.

	OLN						CEL						CEFA					
	SH		2TFB		U		SH		2TFB		U		SH		2TFB		U	
	2008	2009	2008	2009	2007	2008	2008	2009	2008	2009	2007	2008	2008	2009	2008	2009	2007	2008
	Autocorrelation Analysis																	
Min Autocorrelation	-0.21	-0.60	-0.27	-0.25	-0.69	-0.47	-0.23	-0.36	-0.41	-0.24	-0.25	-0.32	-0.20	-0.15	-0.27	-0.27	-0.17	-0.27
Max Autocorrelation	0.54	0.66	0.46	0.58	0.55	0.58	0.44	0.25	0.19	0.40	0.17	0.25	0.31	0.27	0.36	0.39	0.42	0.19
Mean Autocorrelation	0.07	0.00	-0.05	-0.02	-0.01	0.01	0.07	-0.02	-0.03	-0.03	-0.02	-0.01	0.03	0.03	-0.04	0.01	-0.02	-0.01
Absolute Mean Autocorrelation	0.12	0.33	0.16	0.15	0.32	0.26	0.13	0.16	0.11	0.13	0.10	0.15	0.03	0.10	0.12	0.16	0.10	0.11
	Fourier Analysis																	
Vine Spacing (cm)	200		200		180		200		200		180		200		200		180	
Primary Signal Period (cm)	*380*	**190**	290	310	**170**	**190**	**190**	**190**	290	**207**	**170**	**190**	84	**190**	48	67	**170**	*84*
Secondary Signal Period (cm)	253	380	**193**	**207**	52	253	109	95	53	78	76	84	*380*	48	290	150	227	58

Ten of the 18 site-year-metric combinations analysed revealed primary signal periods within 10 cm of the vine spacing (Site A: OLN in 2008 and 2009, CEL in 2008 and 2009, CEFA in 2009; Site B: CEL in 2009; Site C: OLN in 2007 and 2008, CEL in 2007 and 2008, CEFA in 2007). Four of the remaining eight combinations revealed either a primary signal that was reflective of double vine spacing (Site A: OLN in 2008), half vine spacing (Site C: CEFA in 2008), or a secondary signal period within 10 cm of the vine spacing (Site B: OLN in 2008 and 2009).

Spatial structure and sampling efficiency in GOES solutions. The optimal and randomized cluster sampling strategies over a range of sample sizes are shown in Figure 3.4 (site A, 2009 data is presented; other site-year combinations not shown). The optimal sampling strategy, as determined by GOES simulations, resulted in preferential selection of specific clusters at low sample sizes. The preferred clusters are associated with the darker bands in Fig 4B, and are more representative of the

population distribution of CEFA. Conversely, non-preferred clusters which are poorly representative of the CEFA of the population (i.e., outliers) appear as white bands in Fig 3.4A. Optimal cluster sampling locations, as determined by GOES simulations, exhibited strong spatial structure compared to random sampling across all sample sizes, sites, years, and training systems.

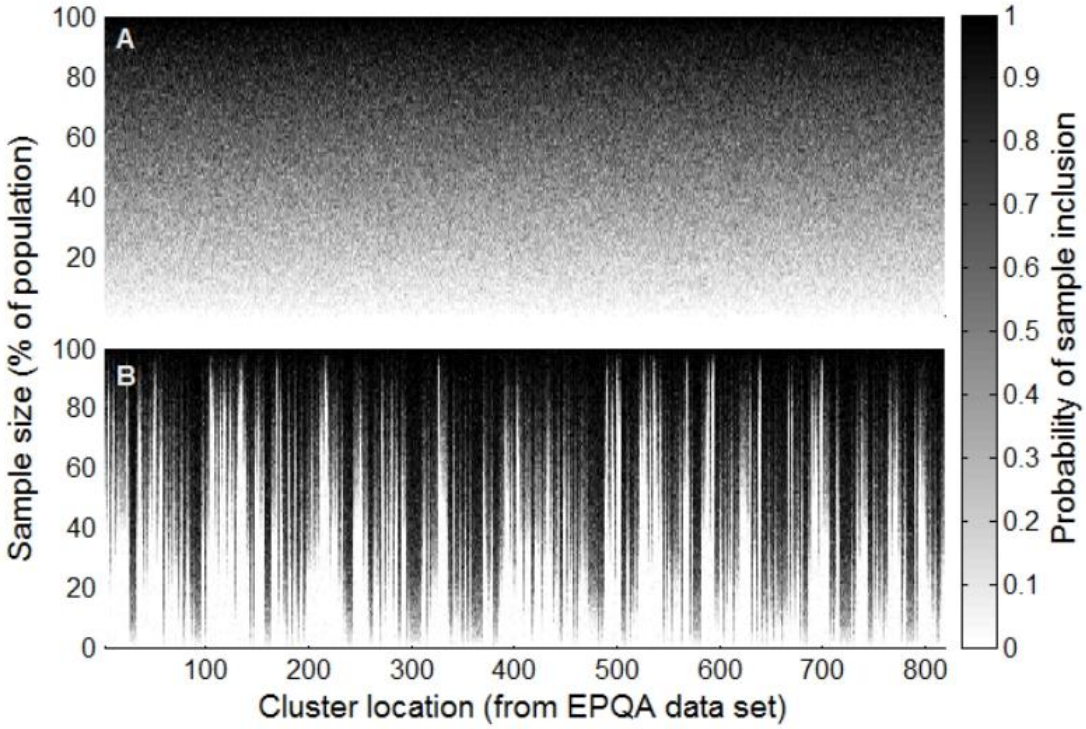

Figure 3.4. Comparison of sampling patterns generated by random sampling (A) and globally optimized spatially-explicit sampling (B) at site A in 2009. Banded pattern in the optimized sample indicates that some clusters (i.e., the dark bands) are preferred over others (i.e., the light bands) when choosing a minimum sample that best represents the targeted population parameters (i.e., the probability distribution of cluster exposure flux availability in the population). Each cluster location on the X-axis corresponds to a specific cluster in an enhanced point quadrat analysis dataset. Each row on the Y-axis represents a sample of size Y%.

When compared to random samples of equal fitness scores, GOES achieved a reduction in sample size vs. random sampling at all sample sizes in all site-year combinations (Figure 3.5), although the extent of the improvement varied among treatments. For operationally practical sample sizes below 20% of the population, GOES resulted in reductions in required sample size ranging from 25% to 60% compared to random sampling (Figure 3.5B).

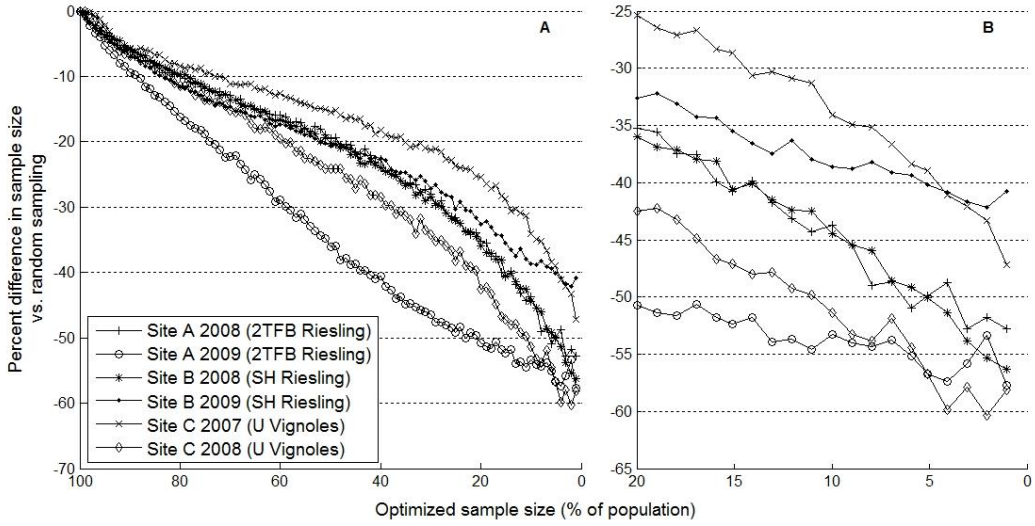

Figure 3.5. Reduction in sample size achieved through spatially-explicit global optimization of sampling. The sample sizes indicated on the X-axis are Y% (i.e., the value on the Y-axis) smaller than a statistically comparable random sample. 2TFB = two-tier flatbow, SH = Scott Henry, U = Umbrella. Sample optimization was performed for cluster exposure flux availability (CEFA). Panel A shows all tested sample sizes. Panel B shows detail of sample sizes between 1% and 20% of population.

Spatial structure and sampling efficiency in STS solutions. Similar to the GOES optimization, the use of a panel weighted template strategy (PW STS) resulted in some panels being preferably sampled over others in the optimal strategy, indicated by the visual banding pattern in Figure 3.6B. Unlike the GOES optimization, a

banding pattern is also visible when clusters are selected at random due to variation in cluster count among panels and thus cluster sampling frequencies (illustrated for site A 2009 in Figure 3.6A; other sites not shown). Similar banding patterns appear for AW STS, reflecting higher cluster count numbers at some positions along the panel than other positions (Figure 3.7A). Visual banding in Figure 3.7B represents the variation in sampling frequencies after being adjusted to the optimal architecture-weighed frequency.

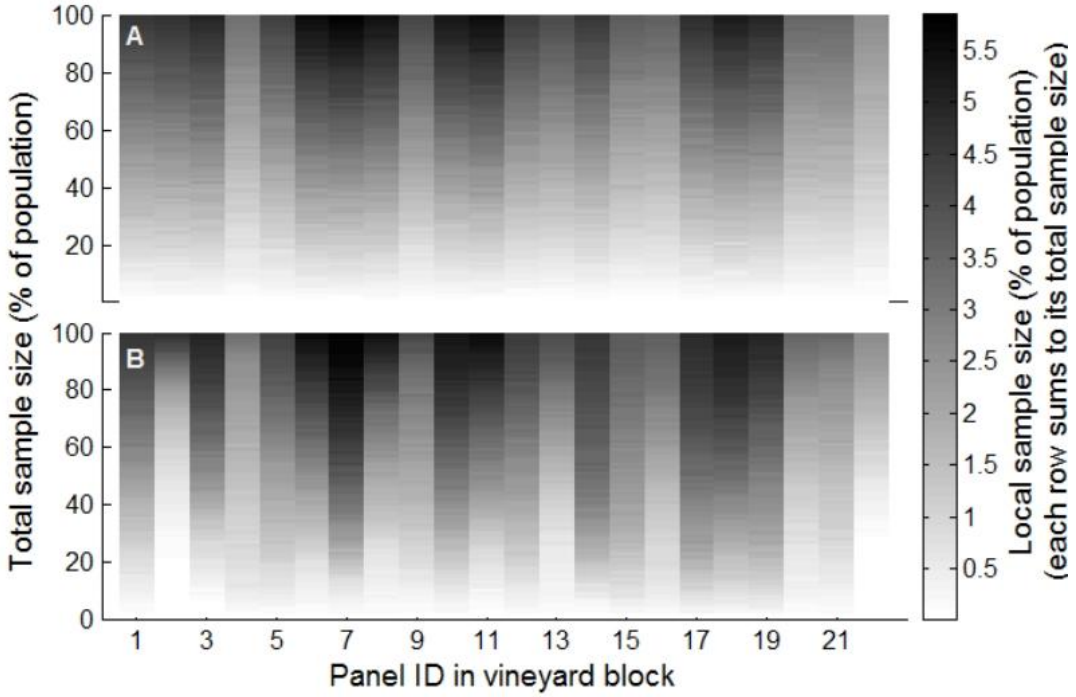

Figure 3.6. Sample density in random (A) and panel-weighted sampling templates (B) (PW STS). Optimized panel-weighted sampling frequencies demonstrating the impact of globally optimized sampling on the probability that a cluster is sampled from each panel (data from Site A, 2009). Visual banding in the random sample plot is caused by variability in cluster count among panels that results in some panels naturally being sampled more than others. Banding differences in the optimized samples are a result of weighting adjustments introduced to improve sample fitness with respect to population parameters.

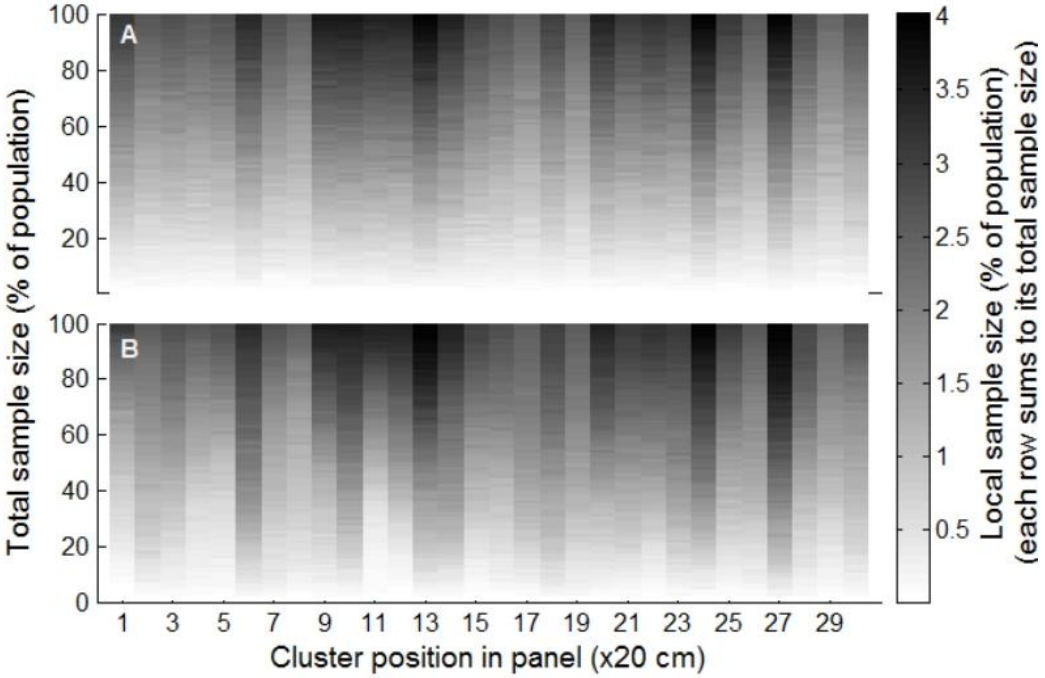

Figure 3.7. Sample density in random (A) and architecture-weighted sampling templates (B) (AW STS). Optimized vine-architecture-weighted sampling frequencies demonstrating the impact of globally optimized sampling on the probability that a cluster is sampled from each position within a canopy panel (data from Site A, 2009). Visual banding in the random sample plot is caused by variability in cluster count among panel locations that results in some locations being sampled more than others. Banding differences in the optimized samples are a result of weighting adjustments introduced to improve sample fitness with respect to population parameters.

When compared to random samples of equal fitness scores, PW STS achieved a reduction in sample size at random-sample sizes below 95% of population in all site-year combinations (Figure 3.8) and reductions varied among treatments. For random sample sizes below 20% of population, PW STS achieved sample reductions ranging from 1% to 24% (plus one outlier of 47%) compared to random sampling. Similarly, AW STS achieved reduction in sample size at random sample sizes below 65% of population in all site-year combinations (Figure 3.9) and reductions varied among treatments. For random sample sizes below 20% of population, AW STS achieved sample reductions ranging from 2% to 21%.

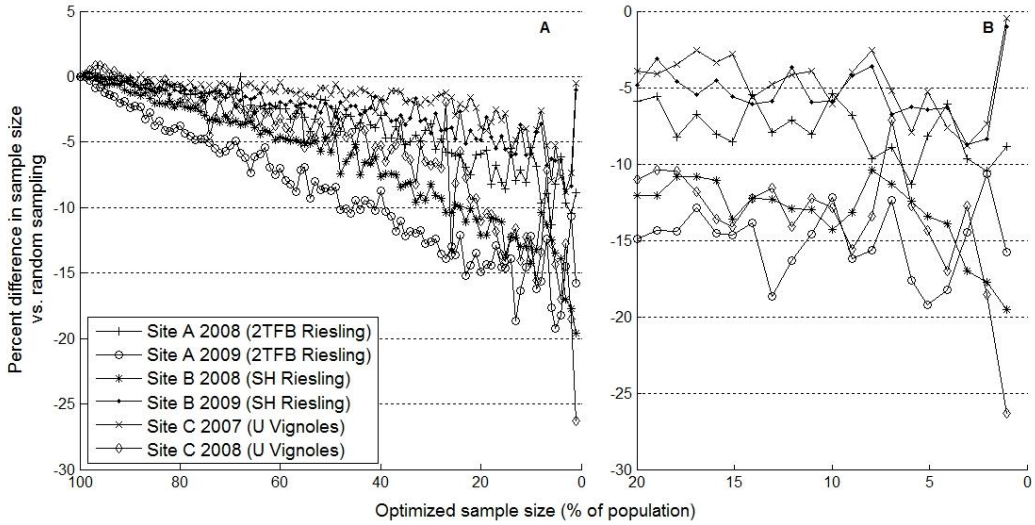

Figure 3.8. Difference in sample size achieved through panel-weighted template sampling. The sample sizes indicated on the X-axis are Y% (i.e., the value on the Y-axis) smaller than a statistically comparable random sample. 2TFB = two-tier flatbow, SH = Scott Henry, U = Umbrella. Sample optimization was performed for cluster exposure flux availability (CEFA). Values below zero represent a reduction in sampling requirements (vs. random sampling), while values above zero indicate an increase in sampling requirements. Panel A shows all tested sample sizes. Panel B shows detail of sample sizes between 1% and 20% of population.

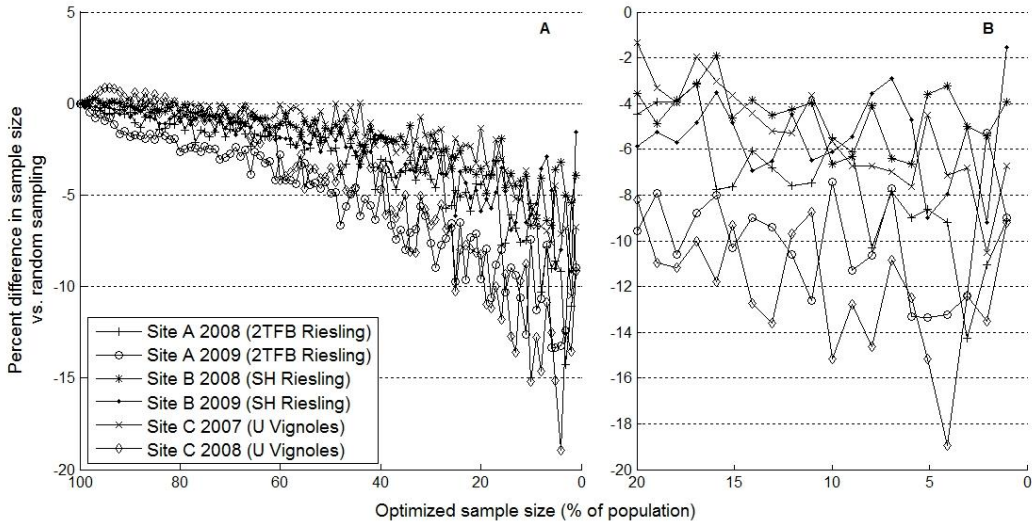

Figure 3.9. Difference in sample size achieved through architecture-weighted template sampling. The sample sizes indicated on the X-axis are Y% (i.e., the value on the Y-axis) smaller than a statistically comparable random sample. 2TFB = two-tier flatbow, SH = Scott Henry, U = Umbrella. Sample optimization was performed for cluster exposure flux availability (CEFA). Values below zero represent a reduction in sampling requirements (vs. random sampling), while values above zero indicate an increase in sampling requirements. Panel A shows all tested sample sizes. Panel B shows detail of sample sizes between 1% and 20% of population.

Discussion

Consistency of structural patterns. Autocorrelation among the reported EPQA metrics (Figure 3.3) suggests that measures of biomass density (OLN) may be more inclined to exhibit periodic spatial patterns than measures of cluster exposure (CEFA, CEL), perhaps due to higher number of leaf contacts vs. cluster contacts per unit of row length, and the efficacy of cultural practices (i.e., leaf pulling) intended to improve exposure consistency. As expected, the vine spacing (180 cm or 200 cm) was similar to either the primary or secondary periods from Fourier analysis (Table 3.1) in nearly all treatments, suggesting that vine spacing is a major factor in controlling spatial patterns in cluster exposure.

Limits of univariate sampling templates. Based on the presence of spatial patterns, and the potential for decreasing sampling sizes by up to 60%, we expected that a sampling protocol based on sample selection at regular locations (AW STS) along the panel should be successful in reducing cluster sample sizes because certain positions would be more representative of the population than others. While AW STS resulted in a reduction in sample size as compared to random selection (up to 21%), the smaller reductions enabled by AW STS compared to both PW STS (up to 24% reduction) and GOES (up to 60% reduction) suggests that the localized three-dimensional structure of a vine row, as influenced by vine spacing, training system, and vine morphology can only partially explain the patterns.

Similarly, while the reduced sample sizes of PW STS compared to random sampling revealed panel-to-panel patterns in field conditions, the additional sample size reductions achieved with GOES as compared to PW STS suggests that those inter-panel patterns do not, in isolation, explain the majority of the spatial structure within the block. Moreover, the ability of GOES to achieve sample size reductions greater than the combined sample reductions from both AW and PW STS suggests that there are additional dimensions, some likely temporal in nature, that must be simultaneously balanced to achieve a reduction in sample size or maximize precision when measuring and describing cluster exposure.

Seasonal stability of spatial patterns. The reduction in sample size requirements for all optimized sampling methods vs. random sampling varied between seasons (Figure 3.5), as did autocorrelation in vineyard parameters and signal period (Table 3.1), suggesting that optimal sampling patterns would differ season to season. While it seems likely that temporal variability in seasonal weather patterns had an effect on season-to-season variability, cultural variability in cane pruning at all three sites may have been a more important factor. Cane positioning, with respect to trunk

location at the vineyard floor, was inconsistent both within a vineyard row and between seasons (data not reported). Individual vines in vineyards in the Finger Lakes region often have several trunks which are trained without deliberate vertical positioning. Recording the location along the panel where a cane (or cordon) meets the fruiting wire could facilitate further analysis and potentially improve season-to-season portability of vineyard maps and sampling solutions. In support of this work, EPQA-CEM Tools (Meyers and Vanden Heuvel, 2008; available from first author upon request) has been updated to allow for the recording of this location, as designated by the letter 'T' which can be added to any EPQA insertion string to denote the location where the cane/cordon meets the fruiting wire.

Economically scalable operational models. The results of the optimized sampling methods demonstrated here suggest a substantial potential for improvement in sampling efficiency, but the practicality of implementation must also be considered. The optimum solution defined by GOES requires locating individual clusters during sampling. While this type of selective harvesting may be justifiable for a researcher, cluster-scale GOES methods are not likely to translate to a commercial vineyard, where sampling is often done by seasonal labour. Ultimately, the increased application of robotic automation in vineyards (Cunha et al. 2010, Morris 2007) may make GOES approaches commercially viable, but the current state of commercial grape production requires a more straightforward and less labour intensive approach toward improving sampling protocols.

PW STS represents an example of an economically customized approach to spatially-explicit vineyard operation. Choosing clusters for sampling at the panel-scale preserves some of the spatial information computed for the best-case GOES solution without the challenge and cost of locating specific clusters. Once CEFA or another parameter of interest (e.g., average estimated berry temperature) is characterized, a

commercial vineyard could then use selective sampling of particular blocks to direct vineyard operations and improve sampling efficiency. Moreover, by using a cluster-scale GOES model as an ideal target, the spatial unit of work within vineyard operations can be scaled up (i.e., moving performance toward logistical simplicity) or down (i.e., moving performance toward the "best-case" sampling scenario) as current labour cost, equipment capability, resource planning maturity, and other economic factors dictate. Architecture based sampling strategies (AW STS) also offered improvements over random sampling, and would be simple to translate into verbal instructions, e.g. "take clusters at 80, 140, and 200 cm from the left edge of each panel". However, the improvements were more modest than those achieved with the block-level based sampling strategies.

Multivariate applications. Although the demonstrated cluster sampling optimization was based on a single ecophysiological parameter (i.e., fruit cluster exposure), heuristic optimization methods more naturally facilitate optimizations across multiple operational objectives. Rather than simply finding the best sampling strategy for representing the population cluster exposure, a multi-objective optimization strategy could balance the influence of additional vineyard parameters. Although collecting the necessary spatial vineyard data for multiple parameters requires an investment in labour and/or technology, continued advances in vineyard sensing technology are likely to improve the economics of data collection through increases in sensor density, sampling frequency, and variety of measureable parameters (Cunha et al. 2010). While the increased application of traditional data processing tools is an obvious response to increasingly larger datasets, the adoption of more sophisticated information processing and operational decision support methods such as those presented here could fundamentally transform vineyard management.

Conclusions

All tested spatially-explicit models reduced required sample size to achieve similar performance as random sampling. Reduction in the required sample size was observed for both panel-weighted (PW STS) and architecture weighted (AW STS) sampling templates, although neither reduction was as great as the best-case globally-optimized sample (GOES). Measurements of cluster exposure have been shown to exhibit varying scales of spatial patterns within a site. Although some patterns can be loosely predicted based on deliberate repetitive cultural practices (e.g. vine spacing or shoot positioning), some are based on less visibly obvious field conditions (e.g. soil structure or slope). Autocorrelation in canopy biomass and fruit exposure was quantitatively linked to fixed vine spacing, but the smaller efficiency gains associated with AW and PW sampling suggest that optimal sampling strategies should simultaneously account for spatial variability at multiple scales. However, even when the underlying cause for the patterns is not definitively known, data from measured spatial patterns can be used to improve operational efficiency by guiding vineyard activities (e.g. sampling or selective harvesting) toward the locations that will most effectively achieve a desired goal. Finally, the methods presented here should be readily applicable to optimizing sampling protocols for other targeted parameters, including multivariate models.

LITERATURE CITED

Acevedo-Opazo, C., B. Tisseyre, H. Ojeda, and S. Guillaume. 2010. Spatial extrapolation of the vine (*Vitis vinifera* L.) water status: a first step towards a spatial prediction model. Irrigation Science 28:143-155.

Bramley, R.G.V. and R.P. Hamilton. 2004. Understanding variability in wine grape production systems 1. Within-vineyard variation in yield over several vintages. Australian Journal of Grape and Wine Research 10:32-45.

Cunha, C.R, E. Peres, R. Morais, A.A. Oliveira, S.G. Matos, M.A. Fernandes, P.J.S.G. Ferreirad, and M.J.C.S. Reis. 2010. The use of mobile devices with multi-tag technologies for an overall contextualized vineyard management. Computers and Electronics in Agriculture 73:154-164.

Glover, F. (1990) Tabu search – a tutorial. Interfaces 20:74-94.

Holland, J.H. 1975. Adaptation in natural and artificial systems: an introductory analysis with applications to biology, control and artificial intelligence (The University of Michigan Press. Ann Arbor, MI).

Iland, P., Bruer, N., Ewart, A., Markides, A. and Sitters, J. 2004. Monitoring the winemaking process from grapes to wine: Techniques and concepts. (Patrick Iland

Wine Promotions, Pty Ltd: Adelaide, SA, Australia).

Jeffreys, H. 1939. Random and systematic arrangements. Biometrika 31:1-8.

Kirk, H.J., F.L. Haynes and R.J. Monroe. 1980. Application of trend analysis to horticultural field trials, Journal of the American Society for Horticultural Science 105: 189-193.

Kasimatis, A.N., E. P. Vilas Jr., F. H. Swanson, and P. P. Baranek. 1975. A study of the variability of `Thompson Seedless' berries for soluble solids and weight. Am. J. Enol. Vitic. 26: 37-42.

Meyers, J.M. and J.E. Vanden Heuvel. 2009. Spatial correlation in vine biomass density suggests need for new design and sampling protocols. Am. J. Enol. Vitic.60:553A.

Meyers, J.M., and J.E. Vanden Heuvel. 2008. Enhancing the precision and spatial acuity of point quadrat analyses via calibrated exposure mapping. Am. J. Enol. Vitic. 59:424-431.

Meyers, J.M., G.L. Sacks, and J.E. Vanden Heuvel. 2009. Naturally occurring spatial variability in canopy biomass impacts flavour and aroma compounds in Riesling. Am. J. Enol. Vitic. 59: 394A-395A.

Morris, J.R. (2007) Development and commercialization of a complete vineyard mechanization system. HortTechnology 14: 411-420.

Rankine, B.C., K.M. Cellier, and E.W. Boehm. 1962. Studies on grape variability and field sampling. Am. J. Enol. Vitic. 13: 58-72.

Reynolds, A.G. and J.E. Vanden Heuvel. 2009. Influence of grapevine training systems on vine growth and fruit composition: a review. Am. J. Enol. Vitic. 60:251-268.

Roessler, E.B. and M.A. Amerine. 1958. Studies on grape sampling. Am. J. Enol. Vitic. 9:139-145.

Student. (1938) Comparison between balanced and random arrangements of field plots. Biometrika 29:363–379.

Tamura, R.N., L.A. Nelson and G.C. Naderman. 1988. An investigation on the validity and usefulness of trend analysis for field plot design, Agronomy Journal 80: 712–718.

Taylor J, B. Tisseyre, R. Bramley, and A. Reid. 2005. A comparison of the spatial variability of vineyard yield in European and Australian production systems. Proceedings of the 5th European conference on precision agriculture. pp. 907–915.

van Es, H.M., C.P. Gomes, M. Sellmann, and C.L. van Es. 2007. Spatially-balanced

complete block designs for field experiments. Geoderma 140:346-352.

CHAPTER 4

IMPACT OF CLUSTER LIGHT ENVIRONMENT ON ORGANOLEPTIC CONCENTRATIONS IN RIESLING

Abstract. Concentrations of organoleptic chemical compounds in Riesling are known to correlate to fruit-zone cluster exposure, although optimal cultural influences with respect to exposure timing and canopy assessment methods have not been established. To explore the spatiotemporal relationships between fruit-zone cluster exposure and harvested concentrations, correlations were measured among eight compounds (glycosylated TDN, β-damascenone, vitispirane, linalool oxide, α-terpineol, 4-vinylguiacol, vanillin, and eugenol), five cluster exposure metrics of varying spatial precision, two sites, and two phenological stages in two consecutive seasons. Pairwise combinations of the cluster exposure metrics (percent interior cluster [PIC], cluster exposure layer [CEL], log(CEL), cluster exposure flux availability [CEFA], and the percent ambient photosynthetic photon flux [%PPF] available at the longitudinal centerline of the fruiting zone), the eight quantified compounds, the two sites, the two phenological stages (fruit set and veraison), and the two seasons (2008 and 2009) resulted in a total of 360 pairwise permutations. Among 22 statistically significant site-year-timing-compound-metric responses, CEFA appeared as the cluster exposure response predictor of highest frequency (8) followed by -logCEL (6), CEL (4), PIC (2), and %PPF (2). Where multiple metrics yielded significant responses for the same site-year-timing-compound combination, a ranking of correlation coefficients among redundant metrics revealed that CEFA was the most frequent best predictor (7 of 12) followed by -logCEL (3 of 12), and %PPF (2 of 12). In comparing

the relative predictive strength among EPQA and PQA metrics, a general pattern emerged: CEFA > log(CEL) $\geq$ CEL > PIC. C13 response data suggested that canopies with low cluster exposure (CEFA < 0.2) may be effective in minimizing the influence of post-veraison cluster exposure on harvested C13 concentrations.

Introduction

Numerous fruit cluster exposure studies have reported correlations between cluster exposure and organoleptically influential secondary metabolites such as phenolics (Downey et al. 2006), monoterpenes (Reynolds et al. 1996, Reynolds and Wardle 1989), norisoprenoids (Kwasniewski et al. 2010, Meyers et al. 2009, Lee et al. 2007), and methoxypyrazines (Ryona et al. 2008, Hashizume and Samuta 1999). Although viticultural treatments such as leaf pulling and shoot thinning are often employed to manipulate fruit exposure, uncertainty remains about quantitative relationships between canopy architecture and organoleptic chemical profiles. Although grape growers desire to control the quality of their fruit, conflicting and inconclusive research data limits their ability to act with decisive precision and economic efficiency.

Many previously reported response studies have utilized point quadrat analysis (PQA) or direct measurement of fruit-zone percent photosynthetic photon flux (%PPF) to characterize cluster exposure; and most have used random subsampling of treatment populations in the measurement of biological responses. In choosing these methods, researchers have made some assumptions about canopy variability. The use of a categorical PQA metric such as percent interior clusters (PIC) or a fixed-location %PPF measurement to quantify cluster exposure, implies that any subtleties in three-dimensional microclimatic spatial structure that may influence variability in cluster exposure can be overlooked in establishing biological responses. Similarly, the use of

random subsampling assumes that canopies are random fields, although recent evidence suggests that neither of these assumptions are valid (Meyers et al. 2010, Meyers et al. 2009).

Although numerous field methods have been demonstrated for quantifying three-dimensional canopy structure (Meyers and Vanden Heuvel 2008, Mabrouk and Sinoquet 1998, Schultz 1995) few are practical for high-volume or low-cost data collection. For example, the method demonstrated by Schultz (1995) is highly precise, but requires an elaborate and obtrusive measurement rigging. The Mabrouk and Sinoquet (1998) method is extraordinarily precise but its destructive sampling and use of complicated imaging tools limits its use to specialized and well-funded research venues. The Meyers and Vanden Heuvel (2008) method, known as enhanced point quadrat analysis (EPQA), offers new field protocols and canopy architecture metrics that improve on the three-dimensional precision of PQA without the need for cumbersome or complicated collection tools.

One EPQA metric, cluster exposure layer (CEL), improves on the spatial precision of PIC and can be calculated from a standard PQA dataset. A second EPQA metric, cluster exposure flux availability (CEFA), uses a computational model to combine PQA datasets and fruit-zone %PPF measurements, thus further improving spatial precision. Contrasting operational cost of these methods, %PPF measurements require an initial investment in a measurement device such as a ceptometer, but subsequently require the least amount of field labor. PIC and CEL require no special field equipment (although calculation of CEL requires access to a personal computer) but requires more labor than %PPF. Calculation of CEFA requires the combined investment in materials and labor of the former metrics.

Organoleptic responses in Riesling. Of particular interest to Riesling is l,l,6-trimethyl-1,2-dihydro-naphthalene (TDN) which imparts a kerosene-like aroma to

finished wines (Simpson 1978). Other C13 norisoprenoids (e.g. beta damascenone which has been demonstrated to enhance fruity aromas) are generally considered to correlate positively with wine quality, but TDN is usually considered to be undesirable (Marais et al. 1992). Due to the combination of TDN's undesirable character, low sensory threshold (Simpson 1978), and responsiveness to fruit exposure, the production of high quality Riesling fruit is dependent on cultural practices that can minimize TDN while, if possible, also maximizing other desirable aroma compounds. In the specific case of managing fruit cluster exposure, quantitative knowledge of dose-response thresholds and other non-linear features would improve the precision of models and the canopy management practices that they guide. This paper seeks to advance the quantitative precision and economic efficiency of methods used to measure and manipulate fruit exposure in viticultural research and commercial production by exploring the relevance of subtle microclimatic structure in the determination of fruit exposure chemical responses of eight chemical compounds while controlling for sampling errors through the elimination of subsampling.

Material and Methods

Vine material. Two Riesling blocks were studied for naturally occurring microclimatic variation at two commercial vineyards (sites 'A' and 'B') in Lodi, NY (Finger Lakes region, east side of Seneca Lake). At site 'A', 72 Scott Henry trained Riesling vines (18 four-vine panels) were selected for consistency (i.e., no missing vines or obviously young replants) from a subplot of 6 rows. At site 'B', 66 Riesling vines (22 three-vine panels) trained to two-tier flatbow with vertical shoot positioning (VSP) were selected for consistency (i.e. no missing vines or obviously young replants) from a subplot of 7 rows. Both sites were planted in north-south row

orientation and managed according to standard viticultural practices for vinifera canopies in the Finger Lakes region. Vine spacing was 2.0 by 2.8 meters and 2.2 by 2.8 meters at sites A and B respectively. Exterior rows and panels were excluded. The experimental unit for a treatment was one panel (i.e., four consecutive vines at site A and three consecutive vines at site B).

Canopy characterization. Point quadrat analysis (PQA; Smart and Robinson 1991), Enhanced point quadrat analysis (EPQA) and calibrated exposure mapping (CEM) were performed at fruit-set (June 27th and July 5th in 2008 and 2009 respectively) and pre-veraison (on August 15thth and August 25th in 2008 and 2009 respectively) by inserting a thin metal rod into the fruiting zone along the transverse axis of the canopy row, as described by Meyers and Vanden Heuvel (2008). A tape measure was used as a guide for insertions, which were made at 20-cm intervals along the length of the four-vine panel at the height of the fruiting wire, resulting in a total of 35 insertions per panel. A Decagon AccuPAR LP-80 photosynthetically active radiation sensor (Decagon Devices; Pullman, WA) was used to measure percent photon flux (PPF). PQA and EPQA metrics were computed for each vineyard panel using Microsoft Office Excel version 12.0.6514.5000 SP2 (Microsoft Corporation; Redmond, WA) and EPQA-CEM Tools version 1.6.2 (available on request from jmm533@cornell.edu).

Weather data. Growing degree day (base 50 degrees Fahrenheit) data were obtained from site-located HOBO weather stations (Onset Computer Corp; Bourne, MA). Precipitation data was obtained from the Network for Environmental and Weather Applications (Cornell University, Ithaca, NY) weather station in Valois, NY.

Cumulative totals were calculated for the ranges between April 15th and fruit-set, between fruit-set and veraison, and between veraison and harvest. Harvest dates in 2008 were October 13th and October 9th for sites A and B respectively. In 2009, fruit was harvested on October 15th at both sites.

Fruit assessment. Panels were individually harvested and pressed in their entirety (i.e. without subsampling), analyzed for soluble solids, treated with 50 mg/L SO_2 and samples (200 ml in 2008; 500 ml in 2009) were frozen at -40C for later analysis. Juice soluble solids were quantified by floating an Ertco 2523PL hydrometer (Nalge; Rochester, NY) in the thawed and pressed juice. Juice samples were thawed at room temperature for approximately 24 hours and analyzed for pH and titratable acidity via titration of 50ml juice samples with 0.1N NaOH on a Mettler-Toledo DL22 auto-titrator and DG115-SC probe (Mettler-Toledo; Greifensee, Switzerland).

Analysis of C13-norisoprenoids, monoterpenes, and phenolics. Targeted organoleptic compounds (glycosylated TDN, β-damascenone, vitispirane, linalool oxide, α-terpineol, 4-vinylguiacol, vanillin, and eugenol) were extracted from juice samples via a solid-phase extraction (SPE) protocol derived from Lopez et al. (2002). Juice samples were thawed at room temperature for approximately 24 hours and centrifuged prior to SPE processing.

4 mL SPE cartridges packed with 200 mg of LiChrolut EN sorbent (Merck KGaA, Damstadt, Germany) were preconditioned with sequential washings of dichloromethane (DCM; 5 mL), methanol (5 mL), and water (10 mL) and loaded with 50 mL of juice at a flow rate of approximately 2 mL/minute via a Cerex SPE processor (Varian, Inc., Palo Alto, CA). Lipids and free volatiles were removed from

the stationary phase with sequential washings of water (4 mL) and a 2:1 v/v mixture of pentane and DCM (7.7 mL). The remaining analyte was eluted with a 9:1 v/v mixture of ethyl acetate and methanol (4 mL) and dried under nitrogen to complete dryness.

Samples were reconstituted with 10 mL of 0.2M citric acid buffer (adjusted with NaOH to a pH of 2.5) and incubated at 100C for 1 hour to hydrolyze the glycosides. 2-octanol was added to the cooled solution to serve as an internal standard at a target concentration of 250 mg/L. A fresh 4 mL SPE cartridge packed with 200 mg of LiChrolut EN was preconditioned with sequential washings of DCM (5 mL), methanol (5 mL), and water (5 mL) and the sample loaded at a flow rate of approximately 2 mL/min. The SPE column was dried under nitrogen for 15 minutes, volatiles eluted with 2.8 mL of DCM, concentrated under nitrogen to a volume of approximately 300 μL, and 100 μL portion drawn for further analysis via GC-MS using a Varian CP-3800 gas chromatograph fitted with a wax column and Saturn 2000 mass spectrometer (Palo Alto, CA). Analytes were identified via retention index and library spectra and quantified relative to the 2-octanol internal standard via ChromaTOF software version 4.22 (Leco Corporation, St. Joesph, MI). Vitispirane peak area was determined through the addition of peak areas for vitispirane A and B. Some monoterpenes were assumed to have been partially rearranged to α-terpineol during acid hydrolysis (Baxter et al. 1978), so α-terpineol was expected to serve as a proxy for total monoterpene concentrations.

Statistical Analysis. Correlation coefficients were calculated for pairwise comparisons among the five metrics of cluster exposure (PIC, CEL, log(CEL), CEFA, and %PPF), eight measured compounds (TDN, β-damascenone, vitispirane, linalool

oxide, α-terpineol, 4-vinylguiacol, vanillin, and eugenol), two sites (A and B), the two canopy measurement timings (fruit-set and veraison) in the two seasons (2008 and 2009) resulting in a total of 320 pairwise permutations. Correlation coefficients were calculated to test responses between microclimatic metrics and fruit composition and also to compare microclimatic metrics as a measure of internal consistency.

Univariate regression analyses were performed for each site-year-compound combination (CEFA vs. relative analyte concentration) at both fruit-set and veraison. Multivariate regression analysis was performed to test the merits of combining fruit-set and veraison measurements and adding crop load, when available, to regressions. Additional model parameters were determined to be insignificant if their individual p values ($Pr > F$) were greater than 0.05. All correlations, regressions and significance tests were performed via SAS version 9.1.3, service pack 4 (SAS; Cary, NC).

Results & Discussion

Growing degree and rainfall accumulation. Total growing degree day accumulation (Figure 4.1) and rainfall (Figure 4.2) were similar in 2008 and 2009, although in 2008 accumulations were weighted toward the latter half of the growing season. In 2008, no additional rainfall occurred during differential harvest dates, so sites A and B are reported with equivalent rainfall accumulations in both years.

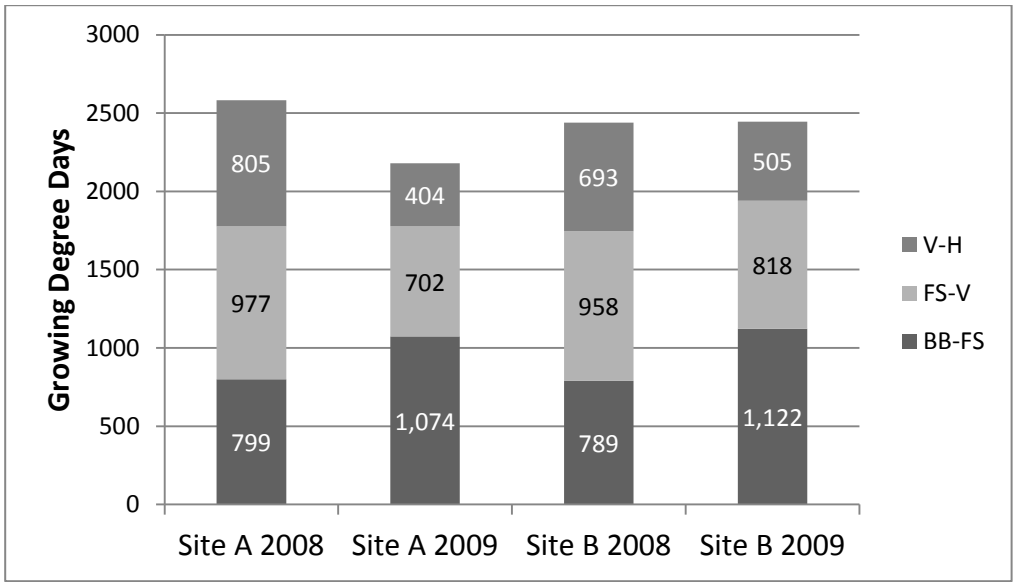

Figure 4.1. Growing degree accumulation (base 50 degrees Fahrenheit) from bud break to fruit-set (BB-FS), from fruit-set to onset of veraison (FS-V), and from onset of veraison to harvest (V-H).

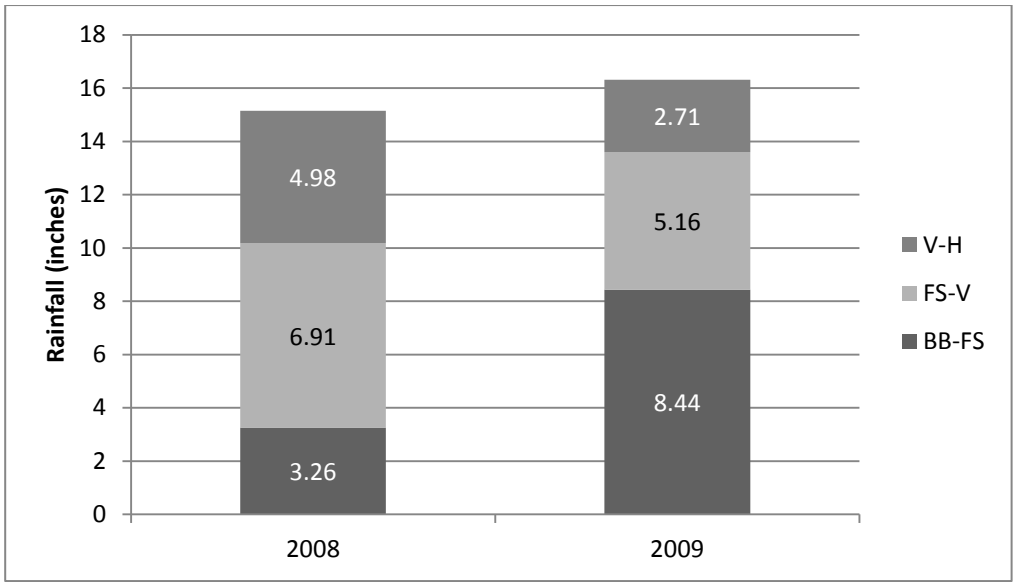

Figure 4.2. Rainfall accumulation from bud break to fruit-set (BB-FS), from fruit-set to onset of veraison (FS-V), and from onset of veraison to harvest (V-H). Sites A and B share data from the same weather station, and no rainfall occurred during differential harvest dates, so sites A and B are reported with equivalent rainfall accumulations.

Correlations between cluster exposure and compound concentrations.

Value ranges of microclimatic indicators (Table 4.1) and relative analyte concentrations (Table 4.2) varied within each site-year combination, suggesting that viticultural practices at both sites were not successful at tightly controlling variability of microclimatic indicators or analyte concentrations. Pearson correlation coefficients of analyte responses (Table 4.3) revealed 22 statistically significant ($p \leq 0.05$) responses representing 12 unique site-year-timing-compound combinations (i.e., some site-year-timing-compound combinations yielded significant responses for more than one cluster exposure metric). TDN responses were most frequent (9), followed by α-terpineol (4), vitispirane (3), β-damascenone (2), eugenol (2) and linalool-oxide (1), 4-vinylguiacol (1), and vanillin (0).

Table 4.1. Ranges, means, and standard deviations of microclimatic metrics. Vines at sites A and B were trained to Scott Henry and two-tier flatbow respectively. PPF = Photosynthetic photon flux at fruit zone. FS = fruit-set. V = veraison. PIC = percent interior clusters, CEL = cluster exposure layer, CEFA = cluster exposure flux availability.

Site	Year	Timing	LLN min-max mean (std)	OLN min-max mean (std)	PIC min-max mean (std)	CEL min-max mean (std)	CEFA min-max mean (std)	PPF min-max mean (std)
A	2008	Fruit set	1.40 - 2.50 2.04 (0.28)	2.00 - 3.18 2.74 (0.34)	50.0 - 84.5 60.8 (10.6)	0.50 - 0.95 0.68 (0.13)	0.13 - 0.40 0.28 (0.07)	6.20% - 48.6% 23.1% (9.38)
		Veraison	1.65 - 2.62 2.08 (0.30)	2.02 - 3.54 2.83 (0.42)	35.2 - 81.4 54.7 (14.7)	0.35 - 0.93 0.61 (0.17)	0.16 - 0.46 0.31 (0.09)	0.50% - 27.00% 5.11% (4.62)
	2009	Fruit set	1.84 - 2.64 2.16 (0.23)	2.14 - 3.19 2.72 (0.29)	66.0 - 94.1 79.0 (9.5)	0.80 - 1.53 1.09 (0.26)	0.03 - 0.21 0.13 (0.06)	0.78% - 28.4% 5.13% (5.09)
		Veraison	1.64 - 2.36 2.05 (0.24)	2.26 - 3.09 2.72 (0.26)	53.1 - 91.2 76.0 (10.3)	0.59 - 1.28 0.99 (0.19)	0.07 - 0.28 0.14 (0.06)	0.51% - 13.03% 1.59% (1.22)
B	2008	Fruit set	1.77 - 3.15 2.42 (0.38)	2.29 - 4.03 3.00 (0.51)	50.0 - 94.8 70.3 (11.4)	0.56 - 1.21 0.83 (0.19)	0.13 - 0.38 0.24 (0.06)	0.70% - 44.7% 9.46% (7.89)
		Veraison	2.90 - 4.33 3.50 (0.43)	4.03 - 5.70 4.67 (0.50)	65.5 - 100 87.8 (8.27)	1.00 - 1.75 1.36 (0.24)	0.06 - 0.20 0.12 (0.04)	0.40% - 11.2% 1.73% (1.62)
	2009	Fruit set	2.71 - 3.85 3.35 (0.31)	3.87 - 5.26 4.52 (0.43)	89.1 – 100 96.1 (3.95)	1.23 - 2.03 1.69 (0.22)	0.03 - 0.18 0.08 (0.04)	0.44% - 17.9% 3.97% (3.88)
		Veraison	2.26 - 3.44 2.78 (0.38)	3.32 - 4.88 4.06 (0.43)	87.9 - 97.6 92.4 (3.54)	1.26 - 1.81 1.47 (0.17)	0.01 - 0.06 0.04 (0.02)	0.51% - 5.05% 1.41% (0.86)

Table 4.2. Relative ranges, means, and standard deviations of analyte concentrations at harvest. Value ranges are arbitrary units derived from GC-MS peak areas vs. and internal standard of 2-octanol. Vines at sites A and B were trained to Scott Henry and two-tier flatbow respectively. ND = Not detected.

Site	Year	TDN min-max mean (std)	Damascenone min-max mean (std)	Vitispirane min-max mean (std)	α-Terpineol min-max mean (std)	Linalool Oxide min-max mean (std)	4-Vinyl Guiacol min-max mean (std)	Vanillin min-max mean (std)	Eugenol min-max mean (std)
A	2008	2.59 – 5.51 3.56 (0.90)	0.44 – 0.97 0.61 (0.16)	0.93 – 2.44 1.52 (0.45)	2.4 – 3.99 3.30 (0.51)	6.78 – 14.88 9.63 (2.41)	10.22 – 77.72 31.32 (22.31)	3.28 – 6.78 4.62 (1.49)	ND
	2009	0.43 - 1.81 1.07 (0.35)	0.04 - 0.14 0.08 (0.03)	0.03 - 0.09 0.06 (0.02)	0.16 – 0.57 0.34 (0.12)	0.21 – 0.67 0.41 (0.13)	0.21 – 1.06 0.54 (0.22)	0.09 – 0.83 0.28 (0.18)	0.03 – 0.18 0.09 (0.04)
B	2008	0.73 – 2.06 1.53 (0.36)	0.03 – 0.90 0.33 (0.20)	0.02 – 0.16 0.08 (0.03)	0.02 – 0.96 0.41 (0.22)	0.18 – 1.40 0.99 (0.26)	0.05 – 3.79 1.02 (0.94)	0.14 – 1.19 0.44 (0.25)	0.03 – 0.28 0.11 (0.06)
	2009	0.75 – 2.42 1.35 (0.48)	0.07 – 0.14 0.09 (0.02)	0.04 – 0.11 0.07 (0.02)	0.21 – 0.68 0.42 (0.12)	0.17 – 1.04 0.54 (0.19)	0.04 – 2.95 0.71 (0.49)	0.11 – 0.96 0.35 (0.18)	ND

Table 4.3. Pearson correlation coefficients for microclimatic metrics versus relative chemical concentrations. †=p ≤ 0.10; *=p ≤ 0.05; **=p ≤ 0.01; ***=p ≤ 0.001. N=9, 24, 33, and 30, for A-2008, A-2009, B-2008, and B-2009 respectively. PPF = Photosynthetic photon flux at fruit zone. FS=fruit-set. V=veraison. PIC=percent interior clusters, CEL=cluster exposure layer, CEFA=cluster exposure flux availability. ND=analyzed for but not detected in more than three treatments.

Metric	Site	Year	Timing	TDN	Damascenone	Vitispirane	Terpineol	Linalool Oxide	Vinyl Phenol	Vanillin	Eugenol
PIC	A	2008	FS	**- 0.69 ***	- 0.45	- 0.40	- 0.42	0.19	- 0.35	0.35	ND
			V	**- 0.80 ***	- 0.62 †	- 0.52	- 0.64 †	- 0.12	- 0.61	0.01	ND
		2009	FS	- 0.05	0.03	0.05	0.11	0.06	0.21	- 0.10	- 0.12
			V	-0.09	0.15	0.18	0.22	0.15	0.20	0.05	- 0.01
	B	2008	FS	0.08	0.04	0.17	0.04	0.07	0.14	- 0.04	-0.04
			V	- 0.16	- 0.02	0.20	- 0.07	0.04	- 0.05	- 0.25	0.46 †
		2009	FS	0.31	- 0.08	- 0.03	0.37 †	0.28	0.33 †	0.39 †	ND
			V	- 0.17	0.21	0.22	- 0.32	- 0.32	- 0.11	- 0.30	ND
CEL	A	2008	FS	**- 0.69 ***	- 0.47	- 0.40	- 0.52	0.16	- 0.43	0.28	ND
			V	**- 0.80 ****	- 0.64 †	- 0.55	- 0.57	- 0.19	-0.60 †	- 0.05	ND
		2009	FS	0.03	0.04	0.07	0.08	0.08	0.26	- 0.18	- 0.13
			V	0.11	0.18	0.18	0.26	0.19	0.14	0.13	0.03
	B	2008	FS	- 0.01	0.02	- 0.07	0.03	- 0.06	0.09	0.03	- 0.10
			V	0.30	0.06	0.31	0.06	0.21	0.04	- 0.16	**- 0.67 ****
		2009	FS	0.33 †	- 0.08	0.16	**0.43 ***	0.36 †	0.32 †	0.32	ND
			V	- 0.24	0.12	0.18	- 0.34 †	- 0.39 †	- 0.13	- 0.25	ND
-log(CEL)	A	2008	FS	**0.70 ***	0.49	0.39	0.56	- 0.11	0.47	-0.24	ND
			V	**0.83 ****	**0.69 ***	0.58 †	0.62 †	0.26	0.62	0.13	ND
		2009	FS	0.01	0.03	0.05	0.06	0.07	0.27	- 0.20	- 0.14
			V	0.08	0.16	0.15	0.22	0.16	0.12	0.11	0.02
	B	2008	FS	0.01	0.05	- 0.06	0.04	- 0.05	0.11	0.07	- 0.07
			V	0.32	0.04	0.35	0.07	0.23	0.03	- 0.16	**0.67 ****
		2009	FS	0.33 †	- 0.11	0.15	**0.41 ***	0.35 †	0.32 †	0.32	ND
			V	- 0.23	0.15	0.20	- 0.35 †	**- 0.40 ***	- 0.12	- 0.25	ND
CEFA	A	2008	FS	0.54	0.59 †	**0.68 ***	0.43	0.00	0.42	0.51	ND
			V	**0.88 ****	**0.73 ***	0.66 †	0.65 †	0.21	0.58	0.09	ND
		2009	FS	0.02	- 0.02	- 0.07	- 0.11	- 0.09	- 0.23	0.12	0.17
			V	- 0.08	- 0.13	- 0.16	- 0.20	- 0.13	-0.19	-0.05	0.06
	B	2008	FS	**- 0.43 ***	- 0.21	**- 0.42 ***	- 0.13	- 0.03	- 0.17	0.00	- 0.20
			V	- 0.18	0.11	- 0.10	0.10	- 0.18	0.15	0.29 †	- 0.46 †
		2009	FS	**- 0.40 ***	0.04	0.03	**- 0.44 ***	- 0.26	**- 0.37 ***	- 0.41 †	ND
			V	0.16	- 0.25	- 0.27	0.31	0.30	0.12	0.30	ND
PPF	A	2008	FS	0.34	0.46	**0.71 ***	0.17	0.14	0.38	0.42	ND
			V	0.44	0.19	0.24	0.29	0.08	0.01	- 0.35	ND
		2009	FS	0.07	0.09	0.01	- 0.02	- 0.01	- 0.05	0.01	0.21
			V	0.20	- 0.01	0.14	- 0.08	0.08	0.09	0.00	0.10
	B	2008	FS	- 0.36	0.32	- 0.30	**- 0.38 ***	0.08	- 0.10	0.02	0.12
			V	0.10	0.16	0.41 †	0.09	- 0.24	0.18	0.12	0.06
		2009	FS	- 0.23	- 0.08	0.02	- 0.26	- 0.07	- 0.22	- 0.18	ND
			V	- 0.17	0.07	- 0.05	- 0.04	- 0.13	- 0.19	- 0.13	ND

Regression analysis of all significant responses (Figures 4.3 through 4.8) revealed generally stronger responses at veraison vs. fruit-set. With the exception of TDN and vitispirane, which responded positively to cluster exposure measured at fruit-set at site A in 2008 (Figure 4.3), all fruit-set responses were negative. However, all negative responses were generally weak (vs. positive responses) with low regression R2 values suggesting that none were biologically significant, leaving only the C13 compounds and eugenol with operationally significant responses. Furthermore, neither C13s nor eugenol consistently responded in all site-year combinations. While C13s responded at both fruit-set and veraison at site A in 2008, no responses were found at site A in 2009, and the responses at site B (all at fruit-set) were weak. Eugenol responded only in one parameter combination (site B veraison in 2008). Multiple regression (combining time points and adding available crop load data) failed to significantly improve any of the regression models ($p > 0.05$ for each of the additional parameters in all cases).

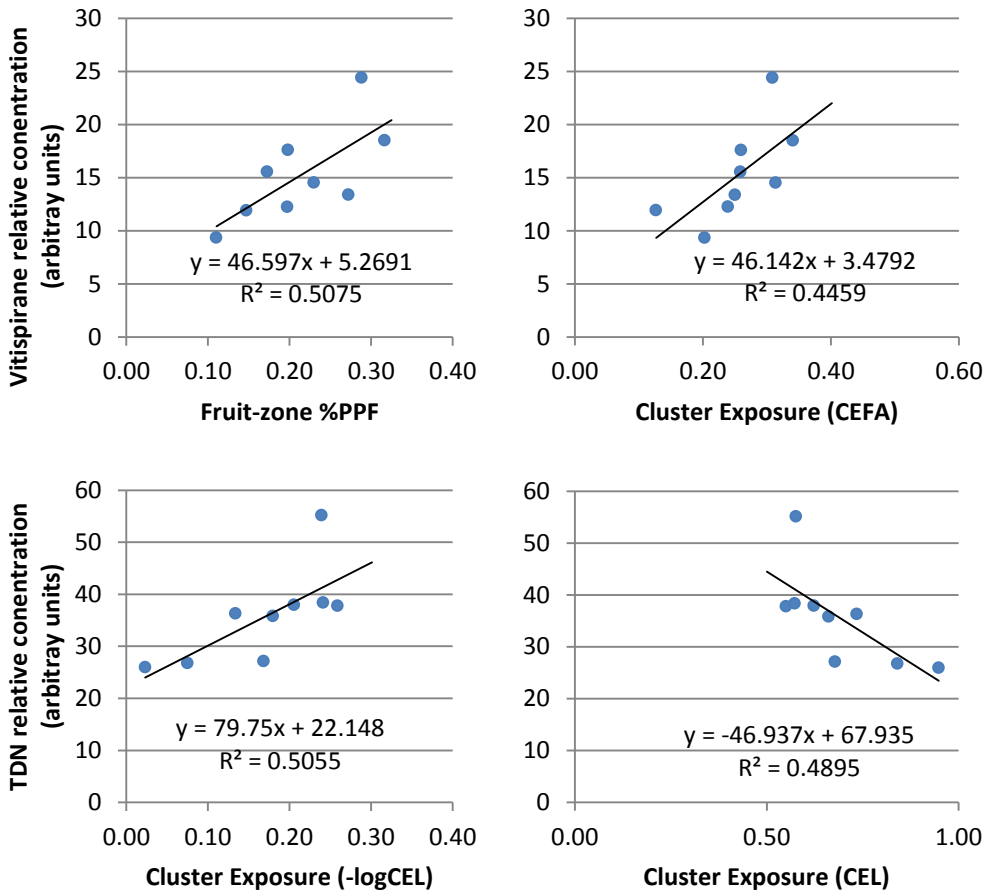

Figure 4.3. Statistically significant responses between fruit-set cluster exposure and analyte concentration at site A in 2008. CEL = Cluster exposure layer. CEFA = Cluster exposure flux availability. %PPF = percent photosynthetic photon flux.

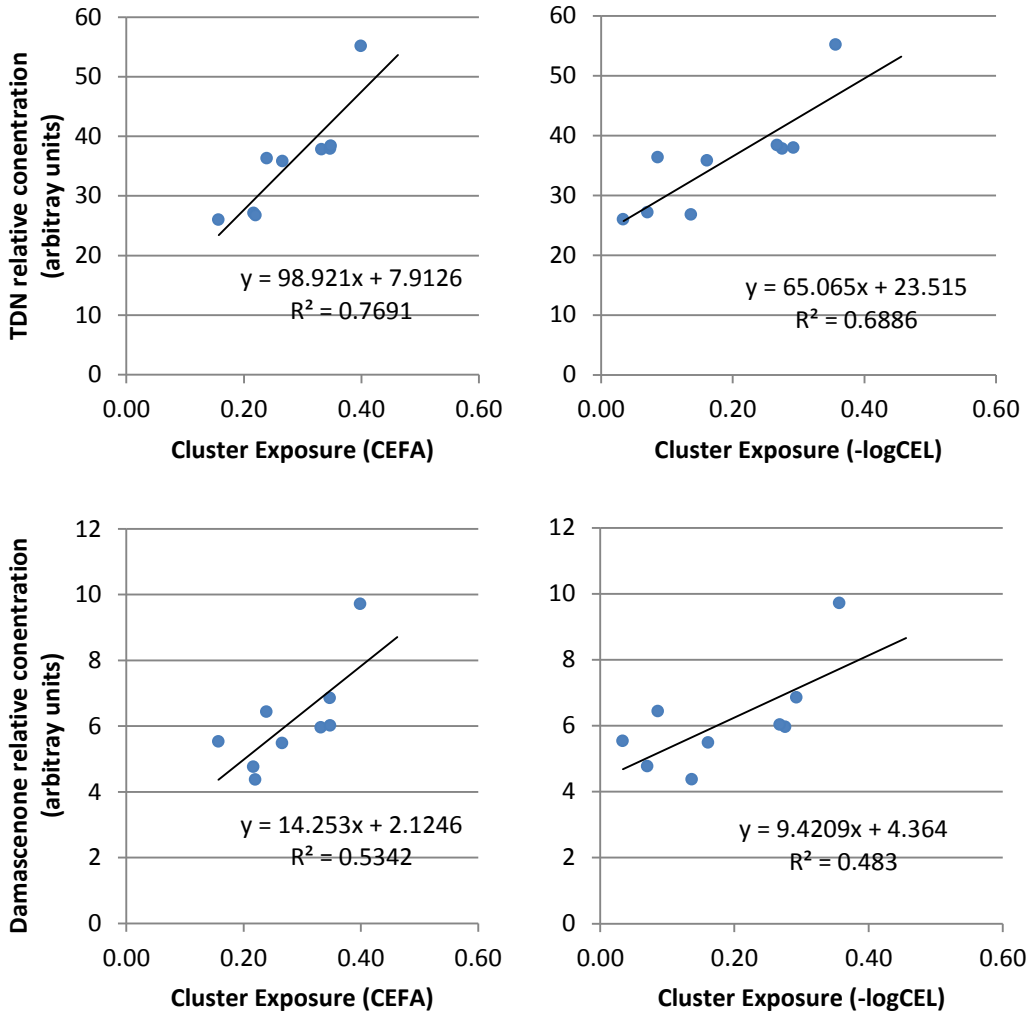

Figure 4.4. Statistically significant responses between veraison cluster exposure and analyte concentration at site A in 2008. CEL = Cluster exposure layer. CEFA = Cluster exposure flux availability.

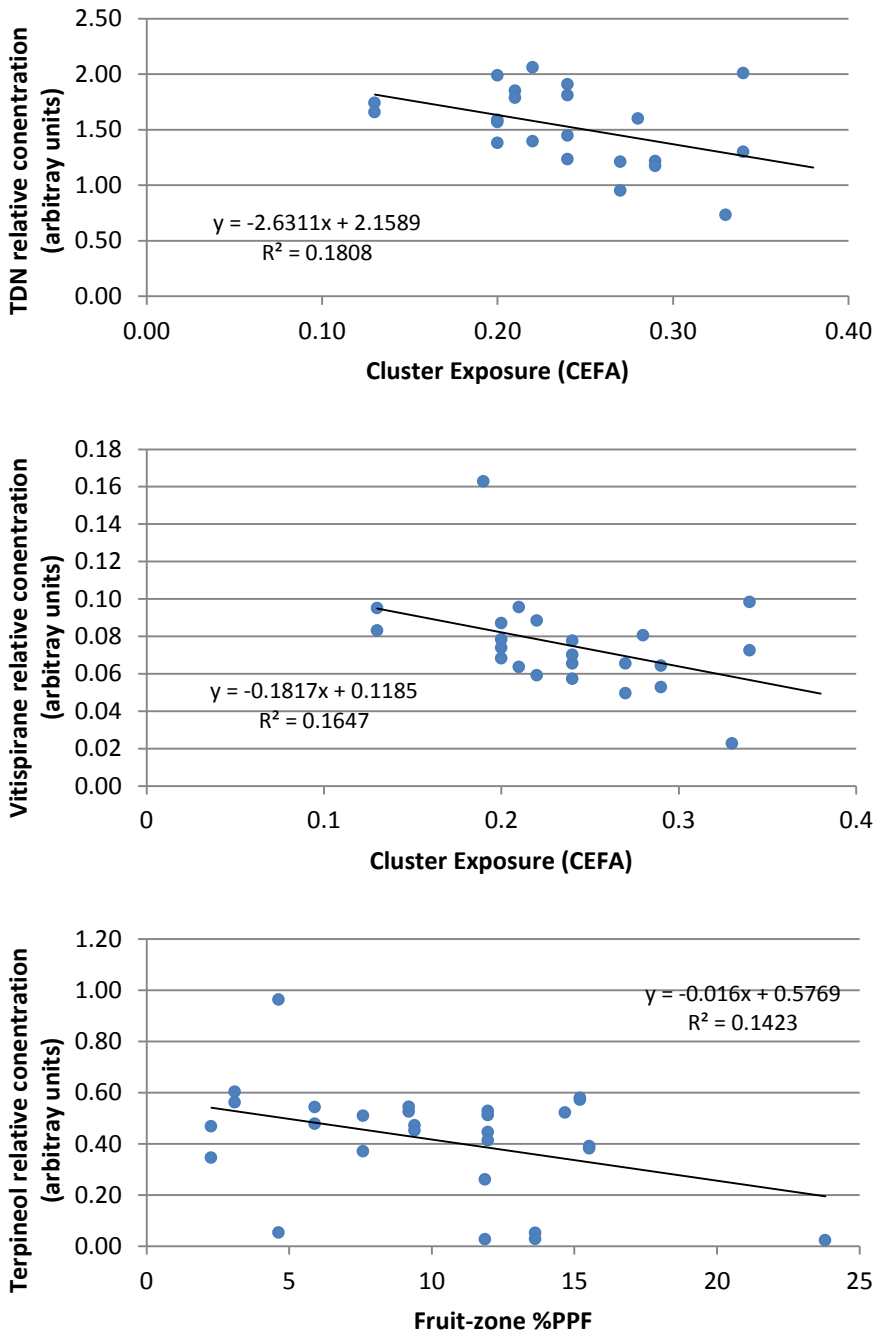

Figure 4.5. Statistically significant responses between fruit-set cluster exposure and analyte concentration at site B in 2008. CEFA = Cluster exposure flux availability. %PPF = percent photosynthetic photon flux.

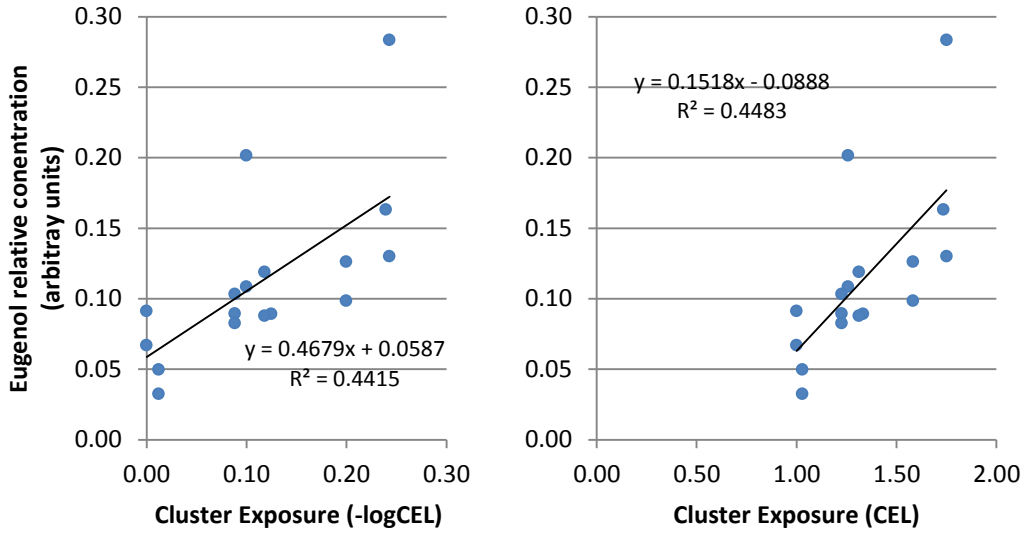

Figure 4.6. Statistically significant responses between veraison cluster exposure and analyte concentration at site B in 2008. CEL = Cluster exposure layer.

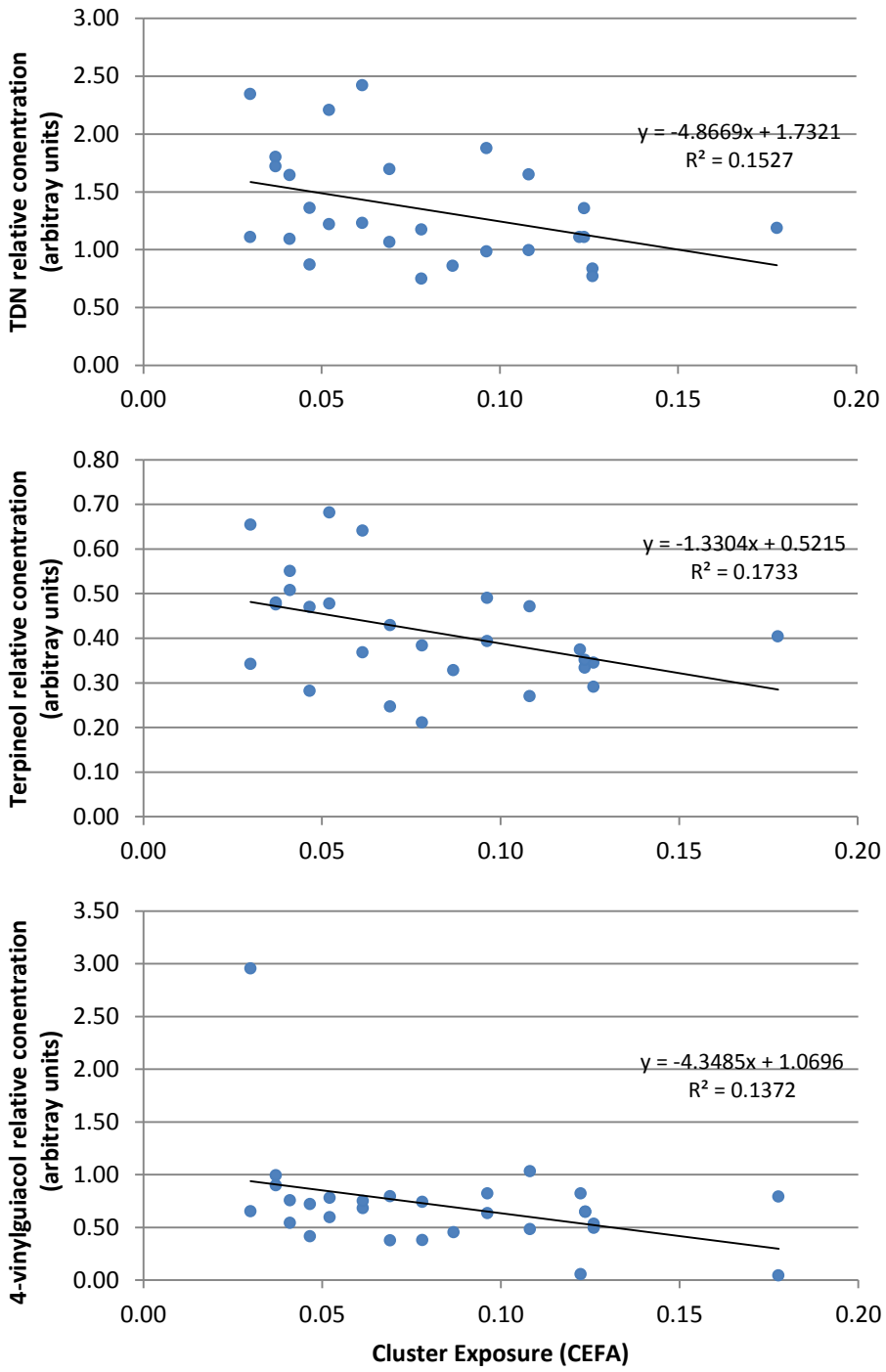

Figure 4.7. Statistically significant responses between fruit-set cluster exposure and analyte concentration at site B in 2009. CEL = Cluster exposure layer. CEFA = Cluster exposure flux availability. %PPF = percent photosynthetic photon flux.

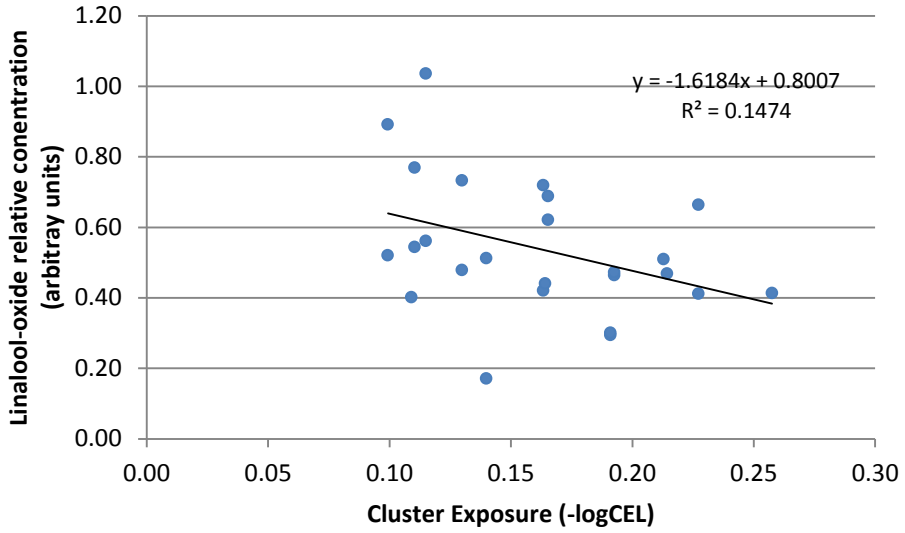

Figure 4.8. Statistically significant responses between veraison cluster exposure and analyte concentration at site B in 2009. CEL = Cluster exposure layer.

A possible explanation for the C13 results is that, although C13s can be expected to respond positively with cluster exposure at both fruit-set and veraison (Kwasniewski et al. 2010), sufficient dose-response thresholds were only achieved at site A in 2008. Previous work on the response of TDN to cluster exposure (Gerdes et al. 2002) has suggested that TDN concentrations in Riesling only respond to fruit-zone sunlight exposures above 20% of ambient sunlight (study was conducted in Davis, CA). Our results appear to be consistent with this assertion in that, in both seasons studied, the average veraison CEFA values at site B (2TFB) were below 0.15 (15% of ambient sunlight) and TDN values were best predicted by fruit set measurements (when fruit was more exposed).

Considering these combined results, it may be reasonable to assume that the final concentrations of C13s in Riesling canopies with veraison CEFA values below 0.20 are independent of post-veraison fruit exposure. However, the comparatively weak responses in 2009 (vs. 2008) could also be attributed to lower post-veraison GDD accumulation. A follow-up time-course study of analyte concentrations could be

helpful in both separating the effects of fruit exposure from seasonal temperature patterns and in measuring the effect of differential harvest dates on the balance between free and bound C13s.

Eugenol in wine is generally assumed to originate from the breakdown of oak-derived lignin (Chatonnet and Dubourdieu 1998). Since the juice samples in this study were not exposed to oak, the positive correlation between cluster exposure and eugenol concentration at site B in 2008 requires a different explanation. In addition to evidence for a broad relationship between sunlight exposure and volatile phenols in wine (Downey et al. 2006), specific evidence of a positive correlation between sunlight intensity and eugenol has been demonstrated in basil (Xianmin et al. 2008). However, the limited evidence presented here does not make a clear case for a relationship between sunlight intensity and the de novo synthesis of eugenol, so the possibility of contamination should also be considered. Preharvest exposure to smoke has been shown to increase eugenol concentrations in juice (Kennison et al. 2008) after acid hydrolysis. Further support for the hypothesis that severity of smoke-taint would correlate to cluster exposure can be found in recent evidence for a positive correlation between fruit sunlight exposure and spray deposition (Austin et al. 2011, in press). However, the lack of evidence for an additional smoke-derived compound response (e.g., 4-methylguaiacol) suggests that a strong conclusion regarding the relationship between cluster exposure and eugenol requires more study.

Best metrics for predicting response. Among the 22 statistically significant site-year-timing-compound-metric responses, CEFA appeared with the highest frequency (8) followed by -logCEL (6), CEL (4), PIC (2), and %PPF (2). Where multiple metrics yielded significant responses for the same parameter combination, a ranking of correlation coefficients among redundant metrics (Table 4.4) revealed that CEFA was the most frequent best predictor (7 of 12) followed by -logCEL (3 of 12),

and %PPF (2 of 12). In comparing the relative predictive strength among EPQA and PQA metrics, a general pattern emerged: CEFA > log(CEL) $\geq$ CEL > PIC. Had this experiment been limited to using only the standard PQA metric for cluster exposure (PIC), only two of the twelve identified unique site-year-timing-compound responses would have been found. In both of these cases, EPQA metrics improved the strength of response. Furthermore, six of the twelve unique responses would not have been missed without the use of a ceptometer (four were found solely using CEFA as the independent variable, one using only %PPF, and one that was found with both CEFA and %PPF). Thus, although EPQA metrics can improve field precision without the use of a ceptometer (using only -logCEL and CEL), performing the canopy calibration needed to calculate CEFA further improves precision and predictive power.

Table 4.4. Ranked predictors of significant biological responses. Primary (1°) predictor is the metric with the strongest correlation coefficient. %PPF = percent photosynthetic photon flux at fruit zone. FS=fruit-set. V=veraison. PIC=percent interior clusters, CEL=cluster exposure layer, CEFA=cluster exposure flux availability.

Site	Year	Timing	Compound	1° Predictor	2° Predictor	3° Predictor	4° Predictor
A	2008	Fruit set	TDN	-log(CEL)	CEL	PIC	--
			Vitispirane	%PPF	CEFA	--	--
		Veraison	TDN	CEFA	-log(CEL)	CEL	PIC
			β-damascenone	CEFA	-log(CEL)	--	--
	2009	Fruit set	--	--	--	--	--
		Veraison	--	--	--	--	--
B	2008	Fruit set	TDN	CEFA	--	--	--
			Vitispirane	CEFA	--	--	--
			Terpineol	%PPF	--	--	--
		Veraison	Eugenol	-log(CEL)	CEL	--	--
	2009	Fruit set	TDN	CEFA	--	--	--
			α-terpineol	CEFA	CEL	-log(CEL)	--
			4-vinylguiacol	CEFA	--	--	--
		Veraison	Linalool-oxide	-log(CEL)	--	--	--

Limitations of ceptometer-based canopy calibration. Although eugenol was found to respond to cluster exposure in one site-year combination (Figure 4.6), CEFA was not a statistically significant predictor for that combination. The superior performance of CEL vs. CEFA in this instance, could be explained the introduction of error during canopy calibration due to limited ceptometer precision at near-zero %PPF values.

Conclusions

Although measures of cluster exposure often strongly correlate among themselves they are not equivalent in their ability to quantitatively predict biological

responses, suggesting that metrics which capture subtle parametric variability, such as CEFA and -log(CEL) are superior predictors of biological response of organoleptic properties and may justify the required investment in equipment and labor. Although extremely low light at the interior of a canopy is typically considered to be undesirable, it appears that it may be effective in minimizing the influence of post-veraison cluster exposure on harvested C13 concentrations in the studied climate which may reduce the need to closely monitor precise cluster exposure post-veraison. In contrast, highly exposed fruit-zone architectures are likely to lead to higher C13 concentrations and efforts to control harvest concentration require closer monitoring of post-veraison cluster exposure.

LITERATURE CITED

Austin, C.N., G.G. Grove, J.M. Meyers, and Wayne F. Wilcox. 2011 (in press). Powdery mildew severity as a function of canopy density: associated impacts on sunlight penetration and spray coverage.

Baxter, R.L., W.A. Laurie, and D. Mchale. 1978. Transformations of monoterpenoids in aqueous acids : The reactions of linalool, geraniol, nerol and their acetates in aqueous citric acid. Tetrahedron. 34(14):2195-2199.

Chatonnet, P., D. Dubourdieu. 1998. Comparative study of the characteristics of American white oak (Quercus alba) and European oak (Quercus petraea and Q. robur) for production of barrels used in barrel ageing of wines. Am. J. Enol. Vitic. 49:79-85.

Downey, M.O., N.K. Dokoozlian, and M.P. Krstic. 2006. Cultural practice and environmental impacts on the flavonoid composition of grapes and wine: A review of recent research. Am. J. Enol. Vitic. 57:257-268.

Gerdes, S.M., P. Winterhalter, and S.Ebeler. 2002. Effect of sunlight exposure on norisoprenoid formation in white Riesling grapes. Carotenoid-Derived Aroma Compounds. Chapter 19, pp 262–272.

Kennison, K.R., G.R. Gibbered, A.P. Pollinitz, and K.L. Wilkinson. 2008. Smoke-derived taint in wine: the release of smoke-derived volatile phenols during fermentation of merlot juice following grapevine exposure to smoke. J. Agric. Food Chem. 56:7379-7383.

Komes, D., D. Ulrich, and T. Lovric. 2006. Characterization of odor-active compounds in Croatian Rhine Riesling wine, subregion Zagorje. Eur Food Res Technol. 222:1-7.

Kwasniewski, M.T., J.E. Vanden Heuvel, B.S. Pan, and G.L. Sacks. 2010. Timing of cluster light Environment Manipulation during Grape Development Affects C13 Norisoprenoid and carotenoid concentrations in Riesling. J. Agric. Food Chem. In press.

Lee, S., M. Seo, M. Riu, J.P. Cotta, D.E. Block, N.K. Dokoozlian, and S.E. Ebeler. 2007. Vine microclimate and norisoprenoid concentration in cabernet sauvignon grapes and wines. Am. J. Enol. Vitic. 58:291-301.

Lopez, R.. M. Aznar, J. Cacho, and V. Ferreira. 2002. Determination of minor and trace volatile compounds in wine by solid-phase extraction and gas chromatography with mass spectrometric detection. J. Chromatogr. (966): 167–177.

Mabrouk, H., and H. Sinoquet. 1998. Indices of light microclimate and canopy structure of grapevines determined by 3D digitising and image analysis, and their relationship to grape quality. Australian Journal of Grape and Wine Research. 4:2-13.

Marais, J., C. Van Wyk, and A. Rapp. 1992. Effect of storage time, temperature and region on the levels of 1, 1, 6-Trimethyl-1, 2-dihydro-naphthalene and other volatiles, and on quality of Weisser Riesling wines. S. Afr. J. Enol. Vitic. 1992, 13:33-44.

Meyers, J.M., G.L. Sacks, H.M. van Es, and J.E. Vanden Heuvel. (Manuscript submitted for review 2010). Maximizing Operational Efficiency via Dynamic Spatially-Explicit Optimization.

Meyers, J.M. and J.E. Vanden Heuvel. 2009. Spatial correlation in vine biomass density suggests need for new design and sampling protocols. Am. J. Enol. Vitic. 60(4): 553A.

Meyers, J.M., G.L. Sacks, and J.E. Vanden Heuvel. 2009. Naturally occurring spatial variability in canopy biomass impacts flavor and aroma compounds in riesling. Am. J. Enol. Vitic. 59(4): 394A-395A.

Meyers, J.M., and J.E. Vanden Heuvel. 2008. Enhancing the precision and spatial acuity of point quadrat analyses via calibrated exposure mapping. Am. J. Enol. Vitic. 59:424-431.

Reynolds, A.G., D.A. Wardle, and A.P. Naylor. 1996. Impact of training system, vine spacing, and basal leaf removal on Riesling. Vine performance, berry composition, canopy microclimate, and vineyard labor requirements. Am. J. Enol. Vitic. 47:63-76.

Ryona, I., B.S. Pan, D. Intrigliolo, A.N. Lakso, G.L. Sacks. 2008. Effects of Cluster Light Exposure on 3-Isobutyl-2-methoxypyrazine Accumulation and Degradation Patterns in Red Wine Grapes (Vitis vinifera L. Cv. Cabernet Franc) J. Agric. Food Chem. 56(22):10838– 10846.

Schultz, H.R. 1995. Grape canopy structure, light microclimate and photosynthesis. I. A two-dimensional model of the spatial distribution of surface area densities and leaf ages in two canopy systems. Vitis 34:211-215.

Simpson, R. F. 1978. 1,1,6-Trimethyl-1,2-dihydronaphthalene: an important contributor to the bottle aged bouquet of wine. Chem. Ind. 1: 37.

Smart, R.E., and M. Robinson. 1991. Sunlight into Wine: A Handbook for winegrape canopy management. Winetitles, Underdale, Australia.

Xianmin, C., P.G. Alderson, and C.J. Wright. 2008. Solar irradiance level alters the growth of basil (Ocimum basilicum L.) and its content of volatile oils. Environmental and Experimental Botany. 63:216-223.